Manuscript Title: Statistical Evaluation of Seismic Velocity Models of Permafrost

Authors: Xiaohang Ji (corresponding author)[1], Ming Xiao[2], Eileen R. Martin[3], and Tieyuan Zhu[4]

[1]Graduate Student, Department of Civil and Environmental Engineering, The Pennsylvania State University, University Park, PA 16802, U.S.A. Email: xhji@psu.edu.

[2]Professor, Department of Civil and Environmental Engineering, The Pennsylvania State University, University Park, PA 16802, U.S.A. Email: mzx102@psu.edu

[3]Assistant Professor, Department of Geophysics and Department of Applied Math and Statistics, Colorado School of Mines, Golden, CO 80401, U.S.A. Email: eileenrmartin@mines.edu

[4]Associate Professor, Department of Geosciences, The Pennsylvania State University, University Park, PA 16802, U.S.A. Email: tyzhu@psu.edu

This paper is a non-peer reviewed preprint submitted to Earth ArXiv.

This paper has been submitted to the Journal Cold Regions Engineering for publication consideration.

Manuscript Title: Statistical Evaluation of Seismic Velocity Models of Permafrost

Authors: Xiaohang Ji (corresponding author)[1], Ming Xiao[2], Eileen R. Martin[3], and Tieyuan Zhu[4]

[1]Graduate Student, Department of Civil and Environmental Engineering, The Pennsylvania State University, University Park, PA 16802, U.S.A. Email: xhji@psu.edu.

[2]Professor, Department of Civil and Environmental Engineering, The Pennsylvania State University, University Park, PA 16802, U.S.A. Email: mzx102@psu.edu

[3]Assistant Professor, Department of Geophysics and Department of Applied Math and Statistics, Colorado School of Mines, Golden, CO 80401, U.S.A. Email: eileenrmartin@mines.edu

[4]Associate Professor, Department of Geosciences, The Pennsylvania State University, University Park, PA 16802, U.S.A. Email: tyzhu@psu.edu

Abstract

The warming climate in high-latitude permafrost regions is leading to permafrost degradation. Estimating seismic velocity in permafrost can help predict the geomechanical properties of permafrost and provide information for planning and designing resilient civil infrastructure in cold regions. Seismic velocities of permafrost are mainly influenced by three components in permafrost: soil grains, water, and ice. Unfrozen water content reflects the variation of ice content and therefore is a key parameter in predicting seismic velocity. This paper statistically evaluates the performance of seven seismic velocity models in predicting seismic wave velocity of permafrost; these models are the time-average model, Zimmerman and King model, Minshull et al. model, weighted equation model, three-phase model, the Biot-Gassmann theory modified by Lee (BGTL model), and Dou et al. model. The unfrozen water content used in these models is obtained from a modified Dall'Amico's model that we propose and this new model is evaluated against six existing unfrozen water content models based on soil temperature. The data used in the evaluation are from published laboratory and in-situ data, including 369 data points for joint P- and S-wave velocities from 9 publications and 980 unfrozen water content data points from 13 publications. This study finds that permafrost of all soil types generally shares the same linear trends between P- and S-wave velocities, regardless of porosity, grain size, and temperature. Fitting all existing data, we derive an empirical linear relationship between P- and S-wave velocities. Among the seismic velocity models evaluated in this study, the Minshull et al. model and BGTL model are the most accurate in predicting seismic velocity of permafrost. The study also provides the applications of seismic velocity models for various permafrost soil types.

Keywords: seismic velocity; permafrost; statistical evaluation; unfrozen water content.

1. Introduction

Increasing air temperatures are driving the warming of permafrost across the high-latitude permafrost regions. As permafrost warms, its geomechanical properties degrade, in turn, permafrost degradation disrupts the natural environment and infrastructure systems and results in long-lasting societal impacts. Studying geomechanical properties of permafrost can help quantitatively understand permafrost warming. The geomechanical properties of permafrost include strength characteristics such as compressive strength, tensile strength, yield strength, shear strength, and dynamic mechanical properties such as bulk modulus, shear modulus, Young's modulus, and Poisson's ratio. The acquisition of these geomechanical properties usually requires accessing and sampling of permafrost using borehole drilling and laboratory testing, which can be difficult, expensive, and time consuming (Ferrero et al., 2014). Observations are limited due to a limited number of sampling sites, while heterogeneity of permafrost leads to potential significant variation of conditions even with a short distance (e.g. near the edge of an ice wedge). Seismic imaging techniques allow us to reconstruct maps of properties in larger regions and identify the heterogeneity of permafrost. Besides, many studies were based on remolded, artificially frozen soil samples, and they may not represent field conditions (Yang et al., 2015). For instance, the shear strength of frozen soil is influenced by sample preparation method, including freezing conditions, strain rate, and sample orientation and size (Radd and Wolfe, 1979). Therefore, to understand the in situ geomechanical properties, in situ measurement techniques are preferred.

Seismic wave velocities estimated using in situ measurements indicate the strength and modulus of soils. Seismic wave propagation is affected by external stresses in permafrost, i.e., compressive, tensile, and shear stresses. Seismic wave velocities are correlated with compressive strength in permafrost (Schön, 2011; Dou et al., 2016). The ultimate compressive strength of permafrost increases with decreasing temperature (Yang et al., 2015; Haynes and Karalius, 1977; Zhu and Carbee, 1984). Besides, yield strength shows a clear correlation with compressive strength (Yang et al., 2015). Laboratory acoustic tests and uniaxial tests were performed to investigate the relationship between seismic wave velocity and peak and residual strength of permafrost (Ferrero et al., 2014).

Bulk modulus, shear modulus, and Young's modulus decrease with increasing temperature (Liew et al., 2022; Yang et al., 2015). Bulk modulus, shear modulus, Young's modulus and Poisson's ratio can be calculated based on seismic wave velocities:

$$K = \rho(V_p^2 - \frac{4}{3}V_s^2) \tag{1}$$

$$G = \rho V_s^2 \tag{2}$$

$$E = \frac{\rho V_s^2(3V_p^2 - 4V_s^2)}{V_p^2 - V_s^2} \tag{3}$$

$$\nu = \frac{V_p^2 - 2V_s^2}{2(V_p^2 - V_s^2)} \tag{4}$$

where V_p is compressional wave velocity, V_s is shear wave velocity, K is bulk modulus, G is shear modulus, ρ is the bulk density of a soil specimen, E is Young's modulus, and ν is Poisson's ratio.

Thus, seismic wave velocities can be used to detect the temporal changes of permafrost, vertical distribution of active layer, permafrost layer, talik formation, distributions of thermokarst and ice wedges, and lateral variability in these features. Apparent increase in seismic velocities in permafrost has been observed as temperature decreases in previous laboratory tests (Nakano et al., 1972; Kurfurst, 1976). The increase primarily coincided with the increase of ice content (Timur, 1968; Nakano and Froula, 1973;

Zimmerman and King, 1986), which is equivalent to the decrease of unfrozen water content (King et al., 1988; Leclaire et al., 1994). Laboratory measurements of acoustic velocities in frozen porous media have shown that P-wave and S-wave velocities sharply increase with decreasing temperature when below 0° C in sandstone samples (King et al., 1988). Therefore, seismic wave velocities can be quantified based on ice content and water saturation. However, quantitatively relating seismic velocities to ice content has proven challenging due to the heavy dependence on the microstructure of ice (Dou et al., 2017).

All seismic velocity models discussed in this study use volumetric proportion of the three permafrost constituents: soil skeleton, water, and ice. The volumetric ice content plays an important role in determining the responses of seismic wave velocity and geomechanical property changes to thermal perturbations (Dou et al., 2016; Dou et al., 2017). Volumetric unfrozen water content can be used to reflect ice content and calculate the volumetric proportion of the constituents. Unfrozen water in frozen soil is a certain amount of liquid water remaining at a negative temperature owing to capillarity and the surface potential energy of soil (Hu et al., 2020). The thermos-hydro-mechanical (THM) behavior of frozen soils is highly dependent on the unfrozen water content (Lyu et al., 2020) and therefore influences the seismic wave velocities and geomechanical properties of permafrost. Unfrozen water content decreases with the decrease of temperature (Watanabe and Osada, 2017). As the unfrozen water content changes, the volume proportions of unfrozen water, ice and soil solid alter and have a strong influence on the mechanics of frozen soil, including seismic wave velocities and geomechanical properties. Measurements of unfrozen water content are usually time-consuming and expensive. Therefore, models for predicting the unfrozen water contents of frozen soils are important.

This paper evaluates seven seismic velocity models corresponding to unfrozen water content. Temperature and total moisture content are first used to determine unfrozen water content. The estimated unfrozen water content of six existing unfrozen water content models is also evaluated statistically. We proposed a modified and simpler unfrozen water content model based on the Dall'Amico's model to provide unfrozen water content estimation in the seismic wave velocity models. The estimated seismic wave velocities of the seven existing seismic wave velocity models are then evaluated statistically. The seven seismic wave velocity models either calculate P-wave or S-wave velocity or composite elastic moduli of permafrost, based on different theoretical assumptions.

2. Reviews of Existing Unfrozen Water Content Models and Seismic Wave Velocity Models Applied in Permafrost

This section reviews existing unfrozen water content models and seismic wave velocity models. Unfrozen water content can be measured using different methods including differential scanning calorimetry (DSC), time domain reflectometry (TDR), nuclear magnetic resonance (NMR), and dilatometer method (Lu et al., 2019). However, these methods are usually time-consuming and expensive (Lu et al., 2019). Therefore, previous research proposed various unfrozen water content models. Section 2.1 reviews six commonly used unfrozen water content models based on soil temperature, including the

Michalowski (1993) model, McKenzie et al. (2007) model, Kozlowski (2007) model, Anderson and Tice (1972) model, Zhang et al. (2017) model, and Dall'Amico et al. (2011) model. Section 2.2 reviews seven existing seismic wave velocity models using estimated unfrozen water content, including the time-average model (Wyllie et al., 1958), Zimmerman and King (1986) model, Minshull et al. (1994) model, weighted equation model (Lee et al., 1996), three-phase model (Leclaire et al., 1994), the Biot-Gassmann theory modified by Lee (BGTL model) (Lee, 2002), and two-end member model (Dou et al., 2017).

2.1 Reviews of Existing Unfrozen Water Content Models in Permafrost

Unfrozen water content is usually calculated based on four parameters: soil temperature, soil temperature and specific surface area of soil particles, soil water characteristic curve, and different types of water (such as free water, capillary water and bound water) (Hu et al., 2020). Evaluation of unfrozen water content models has been conducted by Lu et al. (2019) and Hu et al. (2020). There are two main approaches in the unfrozen water content models: empirical and physical approaches. Among these methods, the models using soil temperatures can be easily applied for seismic wave velocity prediction. This section reviews six commonly used unfrozen water content models based on empirical or semi-theoretical and semi-empirical approaches using soil temperature. Table 1 lists the six unfrozen water content models: Michalowski (1993) model, McKenzie et al. (2007) model, Kozlowski (2007) model, Anderson and Tice (1972) model, Zhang et al. (2017) model, and Dall'Amico et al. (2011) model.

Table 1 Comparison of existing unfrozen water content models (modified based on Lu et al., 2019). All fitting parameters are unitless if not stated.

Models	Formulae and Assumptions	Additional Parameters
Michalowski (1993) model	$$\theta_u = \begin{cases} \theta_{res} + (\theta_0 - \theta_{res}) \exp[\mu(T - T_f)] & T < T_f \\ \theta_0 & T \geq T_f \end{cases}$$ Assumption: The residual unfrozen water content is independent of soil temperature.	θ_u: volumetric unfrozen water content; θ_{res}: residual volumetric unfrozen water content; T: temperature (°C); T_f: temperature of freezing (°C); θ_0: initial volumetric water content at T_f; μ: fitting parameter.
McKenzie et al. (2007) model	$$S_w = \begin{cases} S_{wres} + (1 - S_{wres}) \exp\left[-\left(\frac{T - T_f}{\gamma}\right)^2\right] & T < T_f \\ S_0 & T \geq T_f \end{cases}$$ or $$\theta_u = \begin{cases} \theta_{res} + (\theta_0 - \theta_{res}) \exp\left[-\left(\frac{T - T_f}{\gamma}\right)^2\right] & T < T_f \\ \theta_0 & T \geq T_f \end{cases}$$ Assumption: The residual unfrozen water content is constant.	S_w: unfrozen water saturation; S_{wres}: residual saturation corresponding to the residual volumetric unfrozen water content; S_0: initial water saturation at T_f; γ : fitting parameter.
Kozlowski (2007) model	$$\theta_u = \begin{cases} \theta_{res} & T \leq T_{res} \\ \theta_{res} + (\theta_0 - \theta_{res}) \exp\left[\delta\left(\frac{T_f - T}{T - T_{res}}\right)^{\varepsilon}\right] & T_{res} < T < T_f \\ \theta_0 & T \geq T_f \end{cases}$$ Assumption: The water remains in a liquid form when the soil temperature is above T_f, and the unabsorbed	T_{res}: temperature corresponding to θ_{res}; δ: fitting parameter; ε: fitting parameter.

	water is all frozen when the soil temperature is below T_{res}.	
Anderson and Tice (1972) model	$$W_u = \begin{cases} a(-T)^b & T < T_f \\ W_0 & T \geq T_f \end{cases}$$ or $$\theta_u = \begin{cases} a \cdot \rho_d(-T)^b & T < T_f \\ \theta_0 & T \geq T_f \end{cases}$$ where $$\ln a = 0.5519 \ln S + 0.2618$$ $$\ln b = 0.2640 \ln S + 0.3711$$ Assumption: Adsorptive force governs the freezing of pore water.	W_u: gravimetric unfrozen water content; W_0: initial gravimetric unfrozen water content; ρ_d: dry density of soil; S: specific surface area of soil grains; a: fitting parameter; b: fitting parameter.
Zhang et al. (2017) model	$$\theta_u = \begin{cases} \theta_0 \left[1 - \left(\frac{T_f - T}{T_{k0} + T_f}\right)^{\omega}\right] & -T_{k0} < T < T_f \\ \theta_0 & T \geq T_f \end{cases}$$ Assumption: All liquid water in soil would change into ice if the soil temperature falls below the absolute zero (−273.15 °C).	θ_0: initial volumetric unfrozen water content; T_f: initial freezing point of pore water; T_{k0}= 0 °C; ω: fitting parameter.
Dall'Amico et al. (2011) model	$$\theta_u = \theta_{res} + (\theta_0 - \theta_{res})\{1 + [-\beta\Psi(T)]^n\}^{-(1-\frac{1}{n})}$$ $$\Psi(T) = \Psi_{w0} + \frac{L_{wi}}{gT_f}(T - T_f)$$ Assumption: The residual unfrozen water content is constant.	$\Psi(T)$: soil-water potential energy (m); L_{wi}: the latent heat of phase change between ice and water, L_{wi} = 334 kJ/kg; β: fitting parameter (m^{-1}); n: fitting parameter.

The soil parameters used in the models in Table 1 include water freezing temperature T_f, initial volumetric water content at T_f (θ_0), residual volumetric water content θ_{res}, and soil-water potential energy as a function of temperature $\Psi(T)$. For non-saline soil, T_f =

0 °C is used. Residual unfrozen water content is the unfreezable water content at a low temperature, T_{res}. T_{res} is usually below −10 °C, at which the unfrozen water content is constant or has small changes (Kozlowski, 2007). Soil-water potential energy $\Psi(T)$ is calculated based on the following equation (Dall'Amico et al., 2011):

$$\Psi(T) = \Psi_{w0} + \frac{L_{wi}}{gT_f}\left(T - T_f\right) \tag{5}$$

where Ψ_{w0}= soil-water potential energy related to the total water content and is equal to the soil-water potential divided by $\rho_l g$; ρ_l is density of liquid, g = gravitational acceleration. For saturated soil, Ψ_{w0}=0.

The Anderson and Tice (1972) model, the Michalowski (1993) model, and the Kozlowski (2007) model are initially expressed by gravimetric unfrozen water content. It is converted to volumetric unfrozen water content and shown in Table 1. The relationship between volumetric unfrozen water content (θ_u) and gravimetric unfrozen water content (W_u) is

$$\theta_u = \frac{W_u \rho_d}{\rho_w} \tag{6}$$

where ρ_d is the dry density of soil; ρ_w is the density of water.

Lu et al. (2019) discussed the influence of fitting parameters and the boundary conditions of the Michalowski (1993) model, McKenzie et al. (2007) model, Kozlowski (2007) model, Anderson and Tice (1972) model and Zhang et al. (2017) model. The most common model used is the Anderson and Tice (1972) model, which is a power function relationship between unfrozen water content and negative temperature. However, the model prediction approaches infinity when the temperature is close to 0 °C, making it unreasonable for conditions frequently encountered in polar regions. For the McKenzie et al. (2007) model and the Kozlowski (2007) model with $\varepsilon > 1$ (Table 1), the derivative of the unfrozen water content curve at the freezing point is zero; this means that the unfrozen water content is predicted to remain constant near the freezing point, a behavior that is inconsistent with the actual rapid decrease of unfrozen water content during the freezing process (Lu et al., 2019). Physics-based unfrozen water content models provide more accurate results but are more complicated and difficult to use in practical applications and in numerical modeling (Hu et al., 2020). Physics-based models contain more input properties and requires more computation than empirical models. Some of the properties of soils are difficult to measure, therefore assumptions of the property values are needed. Dall'Amico et al. (2011) model is semi-theoretical and improved from the van Genuchten model (van Genuchten, 1980).

The empirical parameterized unfrozen water content models are easy to implement in numerical modeling with simple formulas. Their limitation is that the fitting parameters lack physical meanings (Hu et al., 2020), and the parameters vary among different soil samples. Meanwhile, theoretical models of unfrozen water content are complicated. Semi-theoretical and semi-empirical models, such as Dall'Amico et al. (2011) model, may mitigate the limitations of the models either entirely based on empirical data or theoretical calculations.

2.2 Review of Existing Seismic Wave Velocity Models in Permafrost

Saturated permafrost is a multiphase porous material that consists of unfrozen water, ice, and soil particles. Permafrost is heterogeneous and discontinuous on a small scale, while seismic wave velocities in permafrost are sensitive to the average properties of a larger scale volume (i.e., wavelength scale) (Guéguen and Palciauskas, 1994; Dou et al., 2017). The seismic wave velocity models discussed in this study assume that the composite density is the volume-weighted average of the densities of the constituents, given by

$$\rho = \phi_w \rho_w + \phi_i \rho_i + \phi_s \rho_s \tag{7}$$

where ϕ_w, ϕ_i, ϕ_s are the volume proportions of unfrozen water, ice, and soil solids, respectively, and $\phi_w + \phi_i + \phi_s = 1$. ϕ_w, ϕ_i, and ϕ_s can be derived based on unfrozen water content, i.e., $\phi_w = \theta_u$, $\phi_i = \theta_0 - \theta_u$, $\phi_s = 1 - \theta_0$ (Table 1).

Three previous studies compared seismic wave velocity models for permafrost (Thimus et al., 1991; Carcione and Seriani, 1998; Lyu et al., 2020). Thimus et al. (1991) and Lyu et al. (2020) used geoacoustic models to determine unfrozen water content. Thimus et al. (1991) made a comparison for Boom clay between the three-phase Wood's equation, time-average equation, and Zimmerman and King (1986) model. Lyu et al. (2020) evaluated eight geoacoustic models relating seismic wave velocity to unfrozen water content and summarized the limitations and applications of each model. Carcione and Seriani (1998) evaluated six seismic wave velocity models, including the Voigt model

(Voigt, 1928), Reuss model (Reuss, 1929), and three-phase Biot theory proposed by Leclaire et al. (1994).

This section reviews the following seismic wave velocity models: time-average model (Wyllie et al., 1958), Zimmerman and King (1986) model, Minshull et al. (1994) model, weighted equation model (Lee et al., 1996), three-phase model (Leclaire et al., 1994), the Biot - Gassmann theory modified by Lee (BGTL model) (Lee, 2002), and two-end member model (Dou et al., 2017). Time-average model, Minshull et al. (1994) model, weighted equation model (Lee et al., 1996), and three-phase model directly calculate P-wave and S-wave velocities, while Zimmerman and King (1986) model and BGTL model calculate bulk and shear modulus and use Equations (1) and (2) to derive P-wave and S-wave velocities. The complete equations of the seismic wave velocity models are presented in Appendix A. Table 2 summarizes the assumptions and applications of these models. The weighted equation model and BGTL model were initially proposed for gas hydrate due to the similarities between frozen soil and gas hydrate (Lyu et al., 2020). Conclusions drawn from hydrate sediment studies should be evaluated before applying to unconsolidated permafrost (Lyu et al., 2020).

(a) Time-average model (Wyllie et al., 1958; Timur, 1968)

The time-average model estimates the effective slowness (i.e., the inverse of velocity) of the multiphase material as the volume-weighted average slowness of the constituents of two-phase material (Wyllie et al., 1958). The model calculates the average time needed for the seismic wave velocity to travel through the material. The assumption is that the

P-wave velocities and transmission coefficients are independent of wave frequencies for elastic media when there is no slippage or separation of interfaces. Therefore, this model is more appropriate for a fully cemented system such as fully frozen permafrost (Lyu et al., 2020). Timur (1968) first proposed a three-phase, time-average equation to explain the compressional wave velocity in various consolidated rocks measured at subzero temperatures. The time-average model can only be used for predicting V_p, but overestimates V_p of permafrost. Therefore, some studies use artificially low P-wave velocity of soil matrix (V_{ps}) (Hoyer et al., 1975; Lee et al., 1996). The model is not applicable if the material is unconsolidated (Wyllie et al., 1958; Dvorkin and Nur, 1998), has clay content or organic content, or contains secondary porosity such as fractures (Timur, 1968; Castagna et al., 1985; Eberhart-Phillips et al., 1989).

(b) Zimmerman and King (1986) model

Zimmerman and King (1986) extended the two-phase wave-scattering theory of Kuster and Toksöz (1974) for estimating three-phase bulk and shear moduli of unconsolidated permafrost (King et al., 1988; Zimmerman and King, 1986). Given that only limited parameters are required, the model was frequently used (King et al., 1988; Kneisel et al., 2008; Lyu et al., 2020). The Zimmerman and King (1986) model assumes unconsolidated permafrost with spherical soil particles embedded in ice-water mixture. The ice-water mixture is composed of spherical water inclusions in a continuous ice phase. The model also assumes a discontinuous water phase in the frozen soil; therefore, only porosity between 30% and 50% and low unfrozen water saturation below 60% can be estimated. This assumption may be invalid for frozen soils with high unfrozen water content.

(c) Minshull et al. (1994) model

The Minshull et al. (1994) model uses a two-end-member mixing approach to derive the seismic wave velocities of permafrost. The Minshull et al. (1994) model constitutes two end members, including fully ice-saturated sediment (fully frozen) as the stiff end member and fully water-filled sediment (fully unfrozen) as the soft end member. The fully frozen end uses the time-average model, and the fully unfrozen end uses Gassmann's equation (Gassmann, 1951). By averaging the two end members, the P-wave and S-wave velocities of partially frozen permafrost can be derived.

(d) Weighted equation model (Lee et al., 1996)

The weighted equation model proposed by Lee et al. (1996) is a modification of the weighted average relationship proposed by Nobes et al. (1986). The model calculates the weighted average of the three-phase time-average model in Section 2.2 (a) (Timur, 1968; Wyllie et al., 1958) and Wood equation (Wood, 1941) of P-wave velocity, initially proposed for hydrate-bearing sediments (Lee et al., 1996). The Wood equation calculates the weighted sum of kinetic energy for constituents of water, ice, and soil solids (Lee et al., 1996; Lyu et al., 2020). The Wood equation can be treated as theoretical minimum value (Lee, 2002) and seems to be more accurate at temperatures near 0 °C for unconsolidated permafrost (Lyu et al., 2020), suitable for high porosity and high water saturation conditions (Lee et al., 1996).

As the elastic properties of ice and gas hydrate are similar (Pearson et al., 1983), the weighted equation model can be applied to permafrost. Empirical parameters W and n are used in the weighted equation model and derived by data fitting. They control the weight of element models and the changing rate of P-wave velocity according to unfrozen water content. Porosity also influences the weight of each element model. Based on Equation A.13, when ϕ decreases, the weight of the time-average model increases.

S-wave velocity V_s in the weighted equation model can be approximately predicted based on an empirical equation for mudrock by Castagna et al. (1985) (Equation A.14). When applying the weighted equation model for permafrost, this empirical linear relationship of P-wave and S-wave velocities may need to be replaced.

(e) Three-phase model (Leclaire et al., 1994)

The three-phase model by Leclaire et al. (1994) is an extension of the two-phase Biot theory, imposing a soil grain – water – ice layered medium structure. The Biot theory describes wave propagation in a statistically isotropic, fully saturated medium with uniform porosity (Biot, 1956; Lyu et al., 2020). The three-phase model assumes no direct contact between solid grains and ice (Leclaire et al., 1994). The model considers the influence of potential energy, kinetic energy and a stress-strain relationship for wave propagation in frozen medium (Leclaire et al., 1994). Due to the strong theoretical basis, it requires many material properties and empirical factors such as soil and hydrate matrix permeability, friction coefficients, and viscosity of free water. These values are difficult or even impossible to measure, and some of them need to be determined by data fitting (Lyu et al., 2020).

There are multiple solutions of P-wave velocities (three solutions) and S-wave velocities (two solutions) based on the three-phase model (Equation A.15 – A.18). Only one of these solutions can be selected as the P- and S-wave velocities of permafrost. While other solutions may mathematically solve these equations, they are physically incorrect and do not fit experimental results.

Carcione and Seriani (1998) evaluated this model using unfrozen water content that mainly considered capillary effect and assumed Gaussian pore size distribution, the values of average pore radius and its standard deviation. In the three-phase model, a percolation model is used to predict elastic moduli of the ice matrix, based on the relationship by De Gennes (1976) and Kuster-Toksöz models (1974).

(f) Biot-Gassmann theory modified by Lee (BGTL model) (Lee, 2002)

Lee (2002) modified the Biot-Gassmann theory (Biot, 1941; Gassmann, 1951) by updating the original two-phase Biot theory, the modified model is named the BGTL model. This model is initially proposed for unconsolidated gas hydrate-bearing sediments (Lee, 2002). The BGTL model considers the effective solid matrix consisting of soil grains and ice based on the Hashin-Shtrikman (HS) average equation (Hashin and Shtrikman, 1963; Hill, 1952).

In BGTL model, Lee (2002) assumed the relationship of P- and S-wave velocities between soil and its solid skeleton are proportional to $(1-\phi_w)$ (Equation A.47) and proposed an empirical relation between the Biot coefficient β and volume proportion of unfrozen water ($\phi_w = \theta_u$) using the weighted equation model (Equation A.48). The later assumption (presented in Equation A.48) is not valid when grains lose contact in high porosity materials. The empirical relationship in Equation A.47 is derived from tested examples of gas hydrate-bearing sediments with ϕ_w in range of 0.19 – 0.68 (Lee, 2002). When the BGTL model is applied to permafrost, Equation A.47 may provide inaccurate Biot coefficient β.

(g) Dou et al. (2017) model

The two-end member model by Dou et al. (2017) is an effective-medium model for saturated, unconsolidated saline permafrost and is an improvement of the Minshull et al. (1994) model. The two end members to form the effective medium of partially frozen sediments include an ice-filled, fully frozen end member and a water-filled, fully unfrozen end member (Dou et al., 2017). Instead of using the time-average model for the fully frozen end as in the Minshull et al. (1994) model (Equations 13 and 14), Dou et al. (2017) used an effective-medium modeling procedure. The fully frozen end uses the self-consistent approximation (Berryman, 1995) and the fully unfrozen end uses the Herz-Mindlin contact theory (Mindlin, 1949) and Biot theory (Dou et al., 2017).

The Dou et al. (2017) model does not require parameter tuning of the mixing proportions and inherently assumes mixed pore-scale ice distributions. However, it overestimates P-wave velocities at moderate to high ice saturations, indicating that the model may overestimate the role of cementing ice at those saturations. Another limitation is that the Dou et al. (2017) model uses modified HS average as mixing strategy, which lacks a physical interpretation.

(h) Summary of the seismic velocity models

A summary of the assumptions and applications of the seismic wave velocity models is shown in Table 2. Some of the models are initially proposed based on other materials such as rock and gas hydrates (e.g., time-average model, Minshull et al. (1994) model, weighted equation model, BGTL model) and applied in permafrost. Some of the models are extended from poroelastic theory, adding assumptions for permafrost (e.g., Zimmerman and King (1986) model, three-phase model). For the time-average model, it calculates the sum of travel time in the individual components and is highly idealized even for rock material. The time-average model is empirical and lacks physical basis. In the application to permafrost, the time-average model can be considered to assume fully frozen permafrost, leading to an overestimation of the seismic wave velocities. An additional limitation of the time-average model is that it can only derive P-wave velocities. The weakness of the weighted equation model and Minshull et al. (1994) model is that the time-average model is a component of these models. The Minshull et al. (1994) model and Dou et al. (2017) model use a two-end-member mixing approach. Both models do not require parameter tuning and incorporate ice and water saturation in the mixing proportion. The improvement of the Dou et al. (2017) model is that it modified the mixing method and replaced the end member models in Minshull et al. (1994) model, avoiding the application of the time-average model. The Zimmerman and King (1986) model and the three-phase model both utilize Kuster-Toksöz equations. The Kuster-Toksöz equations (1974) were initially proposed for two-phase media, commonly used for low-porosity rocks. The three-phase model uses Kuster-Toksöz equations to derive the ice matrix elastic moduli. The Zimmerman and King (1986) model extends the Kuster-Toksöz equations to three-phase permafrost by applying the equations twice. The three-phase model and BGTL model are both extended from Biot theory. The three-phase model imports the phase transition between liquid state and solid state into Biot theory (Leclaire et al., 1994). BGTL model applies Biot-Gassmann equation with Biot coefficient calculated from weighted equation model (Lee, 2002).

Table 2. Assumptions and applications of seismic wave velocity models

Models	**Assumptions**	**Applications**
Time-average model (Wyllie et al., 1958; Timur, 1968)	• Rigid consolidated rock with little fluid • The wave velocities and transmission coefficients are independent of frequencies for elastic media when there is no slippage or separation of interfaces	P-wave velocity of gas hydrates or permafrost (using artificially low matrix velocity for unconsolidated sediments)
Zimmerman and King (1986) model	• Discontinuous water phase in frozen soils • Only considers spherical shape for water and soil phases of unconsolidated permafrost	Permafrost porosities $\phi \in [0.3,0.5]$ and low unfrozen water saturation below 60%

Minshull et al. (1994) model	• Two-end-member mixing approach based on time-average model and Gassmann's equation • Poisson's ratio is independent of porosity	Initially proposed for partially gas-saturated oceanic sediments
Weighted equation model (Lee et al., 1996)	• Weighted average of the three-phase Wood equation and the time-averaged model • Only considers spherical shape for water and soil phases of unconsolidated permafrost	Initially proposed for unconsolidated gas hydrates
Three-phase model (Leclaire et al., 1994)	• Extended based on Biot theory, the corresponding assumptions are statistically isotropic, fully saturated, and with a uniform and connected porosity • No direct contact between solid grains and ice inclusions	Frozen porous media
Biot-Gassmann theory modified by Lee (BGTL) (Lee, 2002)	• Extended based on Biot theory • The V_p/V_s ratio of a consolidated sediment is related to the V_p/V_s ratio of the matrix material and the effective porosity of the soil	Initially proposed for gas hydrates

Two-end member model (Dou et al., 2017)	• Two-end-member mixing approach based on self-consistent approximation and Biot theory	Initially proposed for saturated, unconsolidated saline permafrost

3. Statistical Evaluation of Unfrozen Water Content Models and Seismic Wave Velocity Models in Permafrost

This section evaluates the six unfrozen water content models discussed in Section 2.1 and proposes a modified model based on the Dall'Amico et al. (2011) model (denoted as modified Dall'Amico's model). The modified Dall'Amico's model is then used for the evaluation of seven seismic wave velocity models discussed in Section 2.2. The data used for evaluating the models are collected from published laboratory results. For unfrozen water content models, we collected a total of 66 datasets of unfrozen water content versus temperature with 980 total data points from 13 journal and conference publications. For seismic wave velocity models, we collected a total of 41 datasets of seismic wave velocities (including P- and S-wave velocities) versus temperature with 369 total data points from 9 journal and conference publications. All the datasets are saturated or nearly saturated permafrost. All the soil samples are unconsolidated, non-saline or with low salinity. The dataset's soil index properties are listed in Appendix B.

3.1 Statistical Evaluation of Unfrozen Water Content Models in Permafrost

The 66 datasets of volumetric unfrozen water content with various soil types are plotted in Figure 1, including sand, sand with fines, silt, clay and organic soil. Soils are classified using the Unified Soil Classification System (USCS). The index properties and testing conditions of the soil samples are listed in Table B.1 in Appendix A. More details of the laboratory data could be found in the references (Christ et al., 2009; Li, 2009; Li et al., 2020; Smith and Tice, 1988; McGaw et al., 1983; Oliphant et al., 1983; Aksenov et al., 1998; Hivon and Sego, 1990; Lai et al., 2021; Qiu et al., 2020; Watanabe and Wake, 2009; Zhang et al., 2019; Wen et al., 2012). This meta-analysis indicates that clay (datasets=30 or 45%) is the most tested soil, followed by sand (datasets=16 or 24%), and silt (datasets=9 or 14%). Sand with fines and organic soil is the least tested (datasets=6 or 9%). Fine-grained soils (silt and clay) are the most tested, which is probably due to its capability to hold more moisture and therefore its higher susceptibility to permafrost degradation. As temperature decreases from 0 °C, the decrease rate of unfrozen water content is higher at near 0 °C temperatures and then gradually decreases as temperature further decreases. The changing rate of unfrozen water content is much less at temperatures below -15 °C as compared to the rate of change near 0 °C.

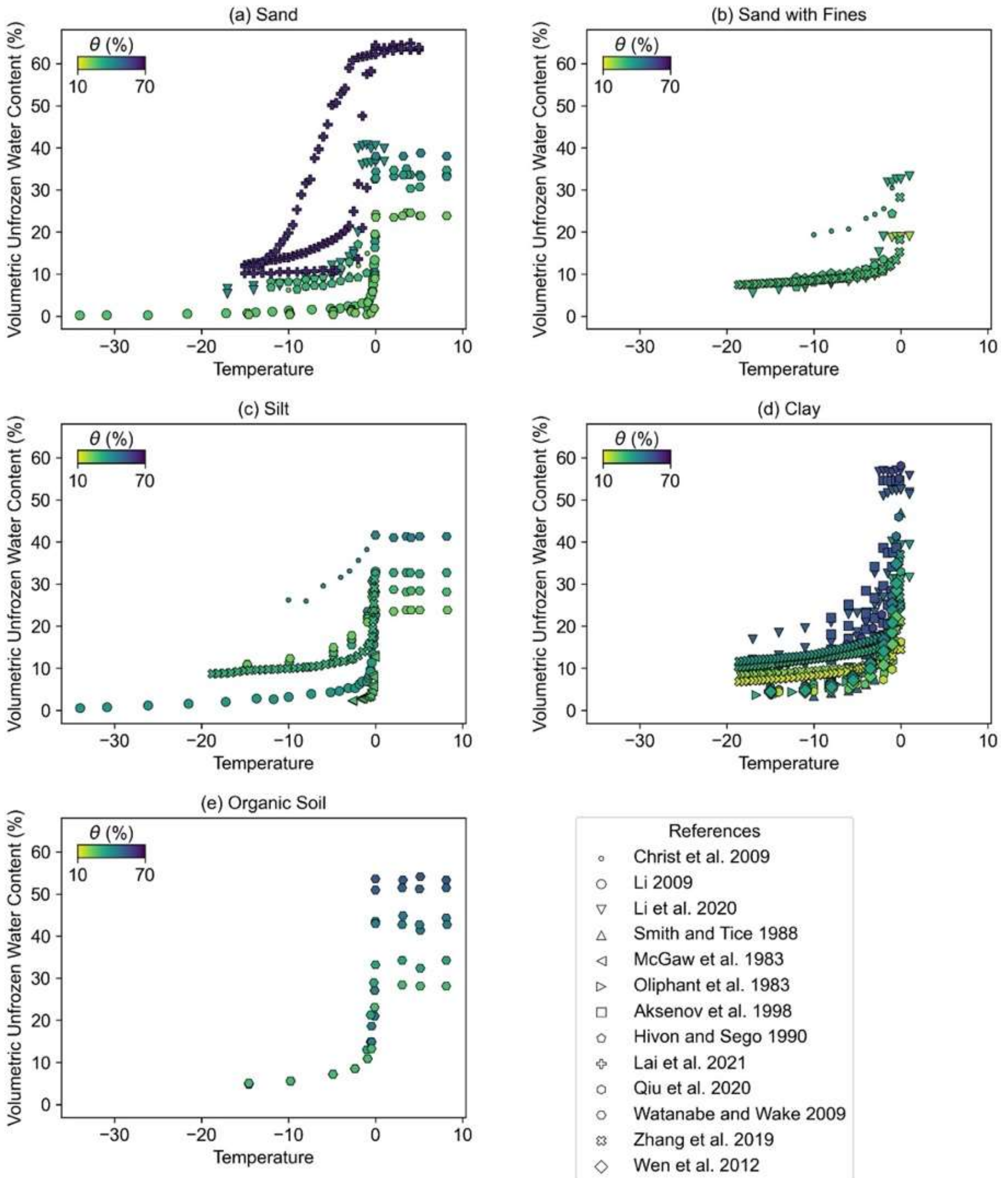

Figure 1. Volumetric unfrozen water content data with temperature

All the unfrozen water content models listed in Table 1 are empirical or semi-empirical. In contrast, the Dall'Amico et al. (2011) model is based on theoretical equations by van Genuchten (1980). The residual unfrozen water content, i.e., the water that cannot freeze even at extremely low temperature, is usually difficult to measure and the estimated values used in practice are based on empirical relationships. Thus, the estimated residual unfrozen water content may not be accurate. Based on the Dall'Amico et al. (2011) model, we propose a modified model assuming that the soil is fully saturated, so that $\Psi_{w0} = 0$, and the residual unfrozen water content is ignored, i.e. $\theta_{res} = 0$:

$$\theta_u = \theta_0 \left\{ 1 + \left[-\beta' \frac{L_{wi}}{g T_f} \left(T - T_f \right) \right]^{n'} \right\}^{-(1-\frac{1}{n'})} \tag{8}$$

where β' and n' are fitting parameters.

We evaluate the modified Dall'Amico model (Equation 8) together with the other six unfrozen water content models discussed in Section 2.1, using root-mean-square error (RMSE) and average deviation. RMSE is the square root of the average of the squared differences between the predicted values and the true values in the dataset. A lower RMSE value indicates that the model makes better predictions on the dataset. The unit of RMSE is the same as the evaluated variable. The average deviation is the mean of predicted values minus measured values and can quantify whether the models are biased to overestimate or underestimate quantities of interest. Figure 2 compares the calculated and measured volumetric unfrozen water contents of the 66 soil samples by the six existing models and the modified Dall'Amico model for different soil types including sand, sand with fines, silt, clay and organic soil. Figure C.1 and C.2 compare the RMSE values and average deviations of the seven models for volumetric unfrozen water content datasets that are grouped by soil types. The overall prediction performances of the Kozlowski (2007) model, Anderson and Tice (1972) model, Dall'Amico et al. (2011)

model and modified Dall'Amico model provide better estimation than the Michalowski (1993) model, McKenzie et al. (2007) model, and Zhang et al. (2017) model. The Michalowski (1993) model and McKenzie et al. (2007) model underestimate θ_u for measured θ_u below 20%. The Michalowski (1993) model underestimates θ_u for sand with measured θ_u above 30%. The McKenzie et al. (2007) model overestimates θ_u for sand and clay with measured θ_u above 30%. Similar performance of the Michalowski (1993) model and McKenzie et al. (2007) model may be due to similar trends in the formulas, with both using an exponential equation and considering residual unfrozen water content. The Anderson and Tice (1972) model provides good performance with the advantage of a simple formula format. The Anderson and Tice (1972) model underestimates θ_u for sand with measured θ_u between 30% and 50%. The Zhang et al. (2017) model was initially proposed for silt. Therefore, the prediction performance of Zhang et al. (2017) model may not predict well for soil types other than silt. Figure 2e shows a general trend that the Zhang et al. (2017) model overestimates θ_u when measured θ_u is less than 25% and underestimates θ_u as measured θ_u increases.

The empirical unfrozen water content models with two fitting parameters perform better than the models with only one fitting parameter. The Michalowski (1993) model has a similar formula format to the McKenzie et al. (2007) model and Kozlowski (2007) model, but the Michalowski (1993) model has one more fitting parameter. As shown in Figure 3a, 3b and 3c, the fitting performance of the Kozlowski (2007) model is better than the Michalowski (1993) model and McKenzie et al. (2007) model. The modified Dall'Amico model has RMSE values similar to Dall'Amico et al. (2011) model. The RMSE values of the modified Dall'Amico model for sand and sand with fines are slightly larger than the values of Dall'Amico et al. (2011) model, while the modified Dall'Amico model (Equation 8) has fewer input properties than the Dall'Amico et al. (2011) model (Table 1). The values predicted by the modified Dall'Amico model for clay samples have a smaller RMSE, indicating better performance than the Dall'Amico et al. (2011) model for clay. For the Kozlowski (2007) model, Anderson and Tice (1972) model and Dall'Amico et al. (2011) model, the predicted volumetric unfrozen water contents match well with the measured values. The modified Dall'Amico model shows a similar overall performance to the Dall'Amico et al. (2011) model. The modified Dall'Amico model has the advantages of a sound theoretical basis, good performance, and suitable amount of input properties. We derive the ranges of the two fitting parameters of the modified Dall'Amico model supported by the fitting results: $\beta' \in (2.49, 3610), n' \in (1.13, 2.72)$. In the following section, the modified Dall'Amico model is used to predict unfrozen water content that is then used as an input for the seismic wave velocity models.

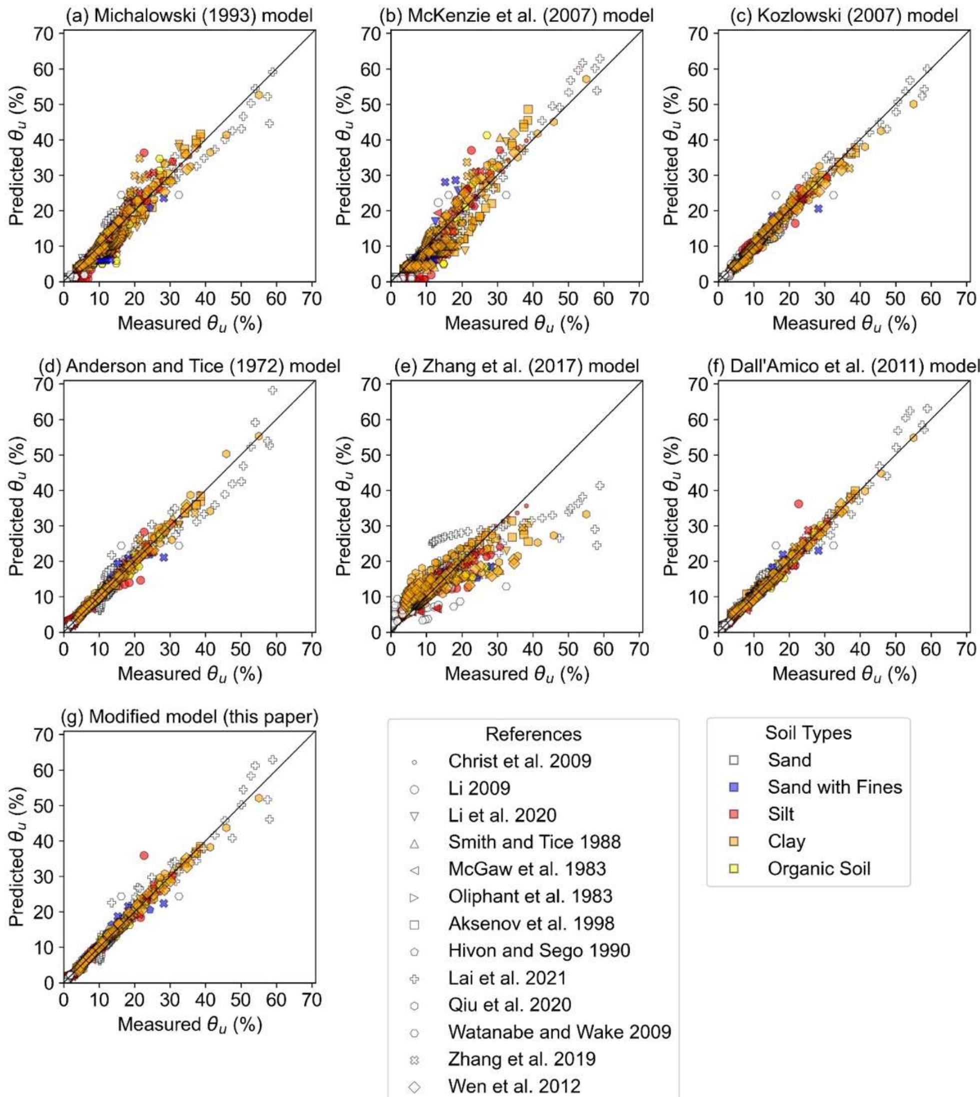

Figure 2. Comparisons between the measured and calculated volumetric unfrozen water contents of the six current models and the proposed model

3.2 Statistical Evaluation of Existing Seismic Wave Velocity Models in Permafrost

This section evaluates seven seismic wave velocity models in permafrost statistically, including the time-average model, Zimmerman and King (1986) model, Minshull et al.

(1994) model, weighted equation model, three-phase model, BGTL model, and Dou et al. (2017) model. The time-average model only predicts P-wave velocities while other six models can predict both P- and S-wave velocities. To evaluate the models of seismic wave velocities, we collected a total of 41 datasets with 369 total data points from 9 journal and conference publications. Table 3 summarizes the number of datasets and data points for each soil type. Soils are classified based on USCS. The number of datasets and data points for each soil type is summarized in Table B.2; the index properties and testing conditions of the soil samples are listed in Table B.3 in Appendix B. More details of the laboratory data can be found in the references (Wang et al., 2006; Christ et al., 2009; Nakano and Arnold, 1973; Kim et al., 2016; Li, 2009; Meng et al., 2008; Fu et al., 1983; Yang et al., 2015; Ge et al., 2013; Zhang et al., 2018). Most of the datasets are non-saline permafrost. Only the datasets from Aksenov et al. (1998) are clay permafrost with low salinity (1 – 15 ppt). The data from the original publications include joint P-wave and S-wave velocities and other elastic moduli: bulk modulus, shear modulus, Young's modulus and Poisson's ratio. All elastic moduli collected in this study are converted to seismic wave velocities based on Equations 1 – 4.

The datasets represent the variations of seismic wave velocities with temperature for various soil types (sand, sand with fines, silt, clay, and organic soil) and are shown in Figures 3 (P-wave velocity versus temperature) and Figure C.3 (S-wave velocity versus temperature). As temperature decreases from 0 °C, the increase rates of P- and S-wave velocities are higher at near 0 °C temperatures and then gradually decreases as temperature further decreases. This trend is consistent with the decrease rate of unfrozen water content as temperature decreases (Figure 1), indicating that the variation of seismic wave velocities is correlated with variation of unfrozen water content. By comparing P- and S- wave velocities of each soil type in Figures 3 and C.3, similar trends can be observed between P- and S- wave velocities.

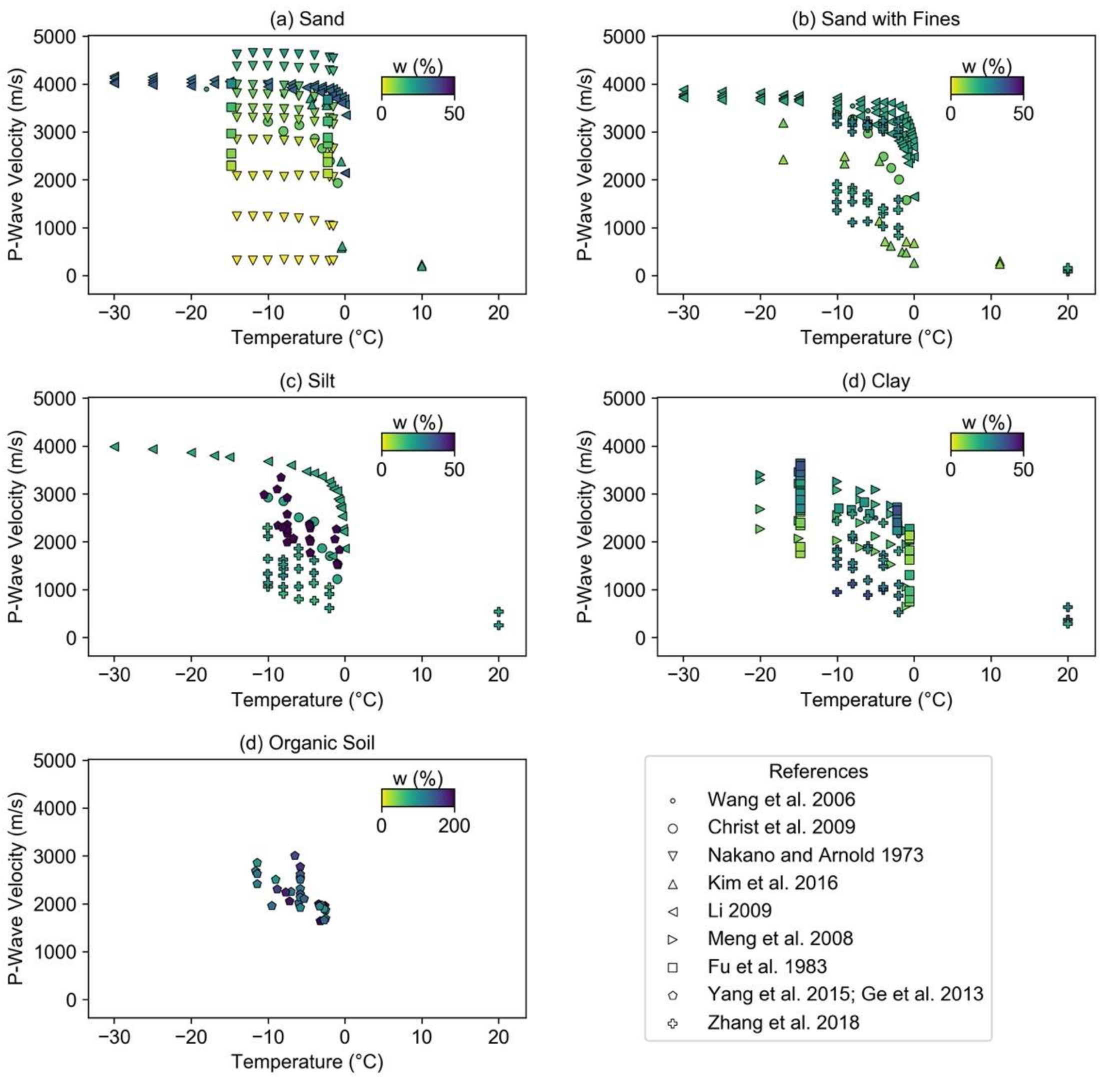

Figure 3. P-wave velocity data of various soils with temperature

The datasets of V_s and V_p in permafrost are plotted in Figure 4; the linear trend shows a clear correlation of V_s and V_p of permafrost. The linear relationship of V_s and V_p coincides with the similar trends of V_s and V_p for all soil types in Figures 3 and C.3.

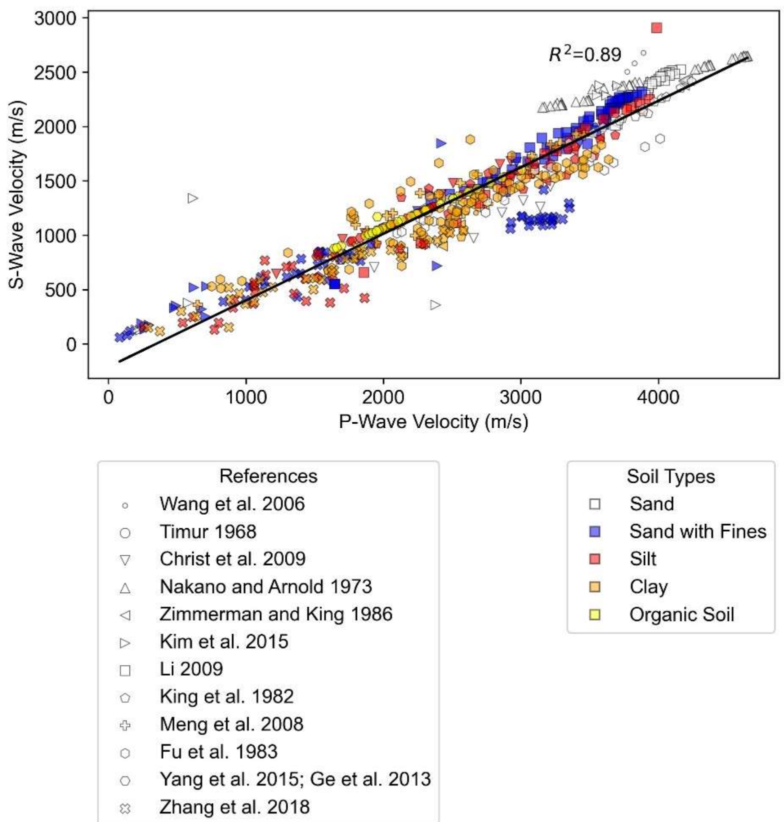

Figure 4. Correlations between P- and S-wave velocities

The following equation shows the linear regression relationship between V_s and V_p in Figure 7, with $R^2 = 0.89$:

$$V_s = 0.6116V_p - 210.4 \quad (9)$$

Equation 9 is applied in the weighted equation model to calculate V_s in this study, as a replacement of Equation A.14. Since Equation A.14 is derived based on mudrock (Castagna et al., 1985), the replacement by equation 9 can increase the accuracy of V_s predictions in the weighted equation model when applied for permafrost. Empirical parameters $W = 1.1$ and $n = 1$ are used in the analysis for the weighted equation model.

The modified Dall'Amico's model (Equation 8) is first used to predict unfrozen water content, which is used as input for the seismic wave velocity models. Therefore, the evaluation results can only represent the performance of the seismic wave velocity models based on predicted unfrozen water content, which may introduce uncertainty of the evaluation results. The applied fitting parameter ranges of the modified Dall'Amico's model in this study are summarized in Table 3 for different soil types, where β' and n' values are selected to make the best fit of seismic wave velocity models.

Table 3 Parameter ranges of the modified Dall'Amico's model for different soil types

Soil Type	β'	n'
Sand (θ_u<40%)	[6, 100]	[1.7, 2.7]
Sand (θ_u>40%)	223	1.57
Sand with Fines	[2.5,10]	[1.2, 1.8]
Silt	[2.5,5]	[1.2, 1.8]
Clay	[1.2, 2.7]	2.5
Organic Soil	4	1.8

The calculated and measured seismic wave velocities of the 41 soil samples are shown in Figure 5 for P-wave velocities and Figure 6 for S-wave velocities. Values used for elastic moduli and densities are shown in Table B.4. Figures C.6 – C.9 compare the RMSE values and the average deviations for different models for P- and S-wave velocities, respectively, for different soil types. The prediction results from different seismic wave velocity models depend on their theories and assumptions. The performance of the models varies even for the same soil type. For example, in Figure 5 and Figure 6, the predictions of sand with fines for the dataset by Kim et al. (2016) are higher compared with other datasets of sand with fines. This is likely because the testing method in Kim et al. (2016) was resonant column test, different from other samples' testing method, which may affect the microstructural distribution of pore ice in the sample. The performance of the same model varies for different soil types. This indicates that different seismic velocity models should be used depending on permafrost soil types. The performances of the six models' S-wave velocity predictions differ in their performances for P-wave velocity prediction because of different methods for S-wave velocity predictions, including calculating from composite shear modulus (most common), direct theoretical calculation, and empirical relationships between P- and S-wave velocities.

For all soil types, the time-average model and weighted equation model mostly overestimate P-wave velocities. For the time-average model, this is due to the assumption of fully frozen state of permafrost, while unfrozen water exists in permafrost. Among the seven seismic wave velocity models, this can be treated as the upper-bound prediction. The performance of the weighted equation model is similar to the time-average model since the weighted equation model uses the input from the time-average model. The empirical equation of Biot coefficient β (Equation A.48) in the BGTL model is derived based on the weighted equation model, while the performance of the BGTL model is better than the weighted equation model. The weighted equation and BGTL models have acceptable prediction for silt, clay and organic soils when V_p is less than 3000 m/s; however, they overestimate V_p and V_s for sand with fines as shown in Figure 5d and Figure 6e. The prediction of the three-phase model is relatively accurate when V_p is between 2000 m/s to 3000 m/s, while overestimates when V_p is less than 2000 m/s and underestimates when V_p is larger than 3000 m/s. The three-phase model performs better for sand and sand with fines, while overestimates fine-grain soils including silt, clay and organic soil. The overestimation of V_p in the three-phase model when V_p is less than 2000 m/s may be due to the assumption of no direct contact between solid grains and ice inclusions. This assumption works well for negative temperature near 0 °C when permafrost is close to unfrozen state, but not for lower temperature as ice content increases, likely due to the complex contact among soil skeleton, unfrozen water and ice and the effects of diffuse double layer and different microstructure of ice. V_s of the three-phase model is underestimated for sand and sand with fines.

Note that the time-average model can only predict V_p with an overestimation. Overall, the seismic wave velocities calculated by the Minshull model, Dou et al. (2017) model and BGTL model match better with the measured data than other models. While with V_p decreases, the bias of the Dou et al. (2017) model increases. For the Zimmerman and King model, the prediction for sand with fines shows better accuracy than for other soil types. The BGTL model preforms better for sand compared with other models. For V_p of silt, the three-phase model shows lower RMSE values, while the Zimmerman and King model shows larger RMSE values.

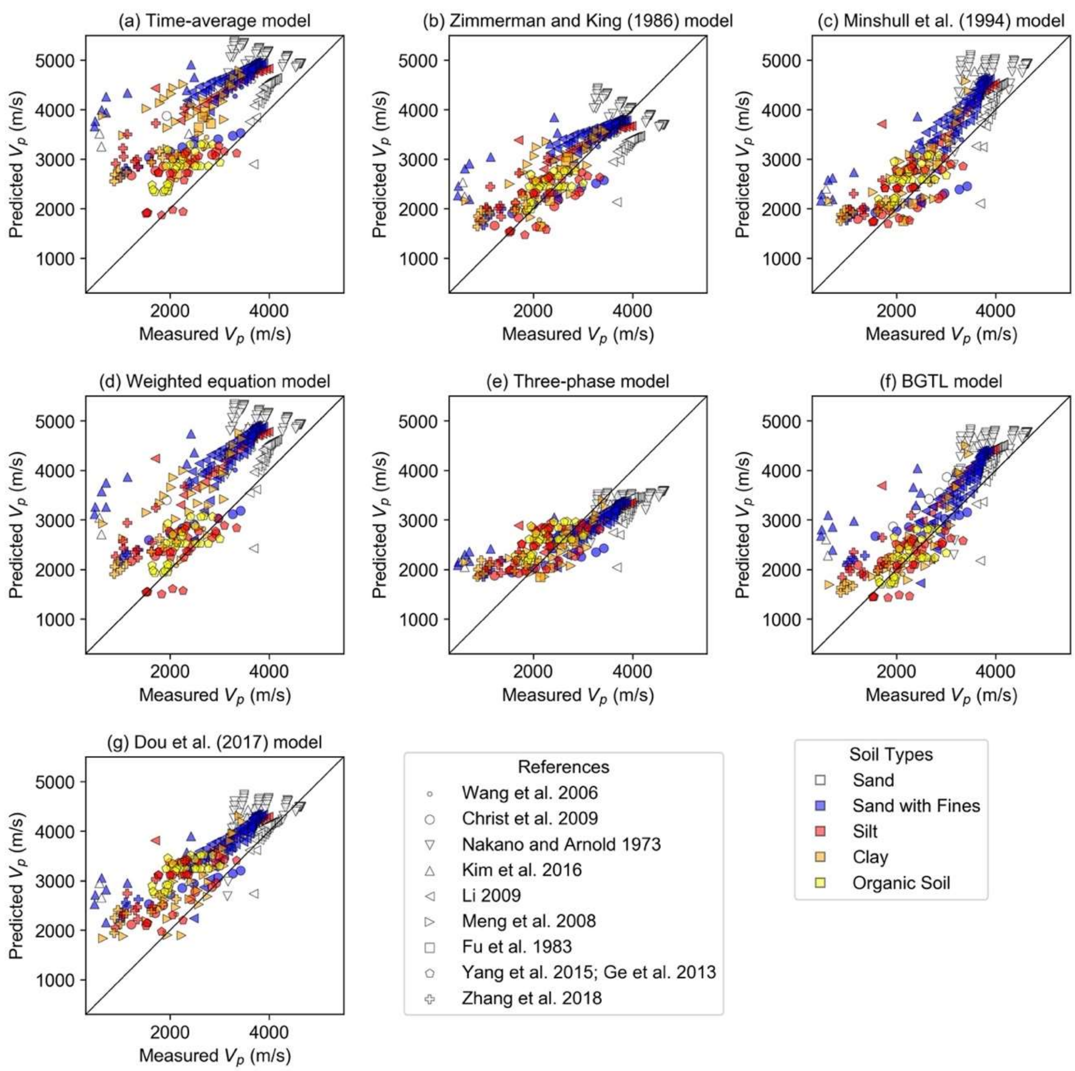

Figure 5. Comparisons between the measured and calculated V_p

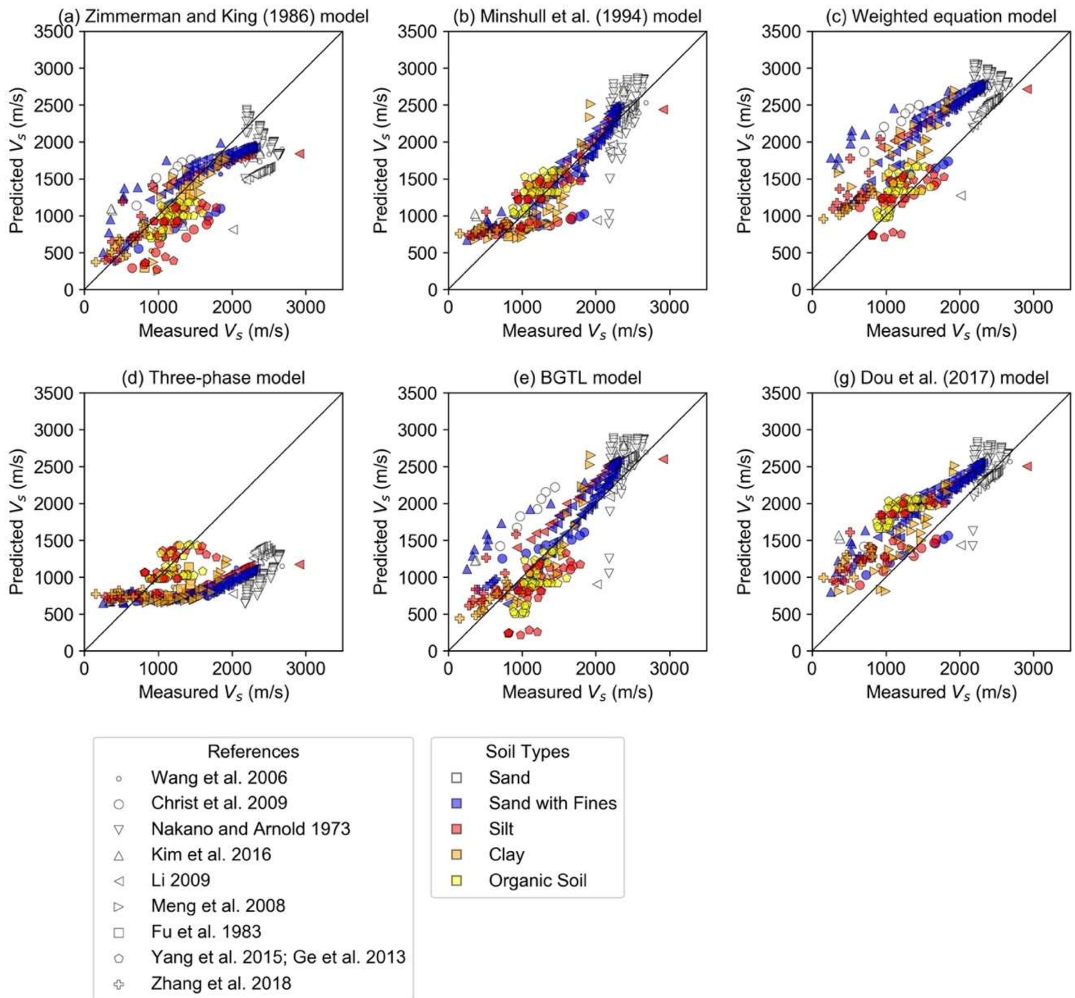

Figure 6. Comparisons between the measured and calculated V_s

4. Discussions

We compared and evaluated the unfrozen water content models of different soil types. We proposed a modified Dall'Amico's model (Equation 8) to predict unfrozen water content of permafrost. The modified Dall'Amico's model is a semi-theoretical and semi-empirical model based on soil temperature and assumes that the permafrost is fully saturated, and the residual unfrozen water content is zero. Determining the residual unfrozen water content is difficult and requires specific surface area and diffuse double layer thickness of clay soils (Saarenketo, 1998). For practical use, the assumption of zero residual unfrozen water content may change the fitting parameter values but has little influence on the prediction accuracy. The modified Dall'Amico's model needs one variable and two fitting parameters and is simplified for practical purpose. The regression analysis shows similar prediction accuracy compared to the original Dall'Amico's model.

The prediction of all unfrozen water content models shows overall good performance. This is because all unfrozen water content models reviewed and evaluated in this study use fitting parameters. However, the disadvantage of this kind of model is the determination of fitting parameters when applying the models to a sample without unfrozen water content measurements. Based on the RMSE results in Figure C.1, unfrozen water content models with two fitting parameters perform better than models with one fitting parameter. The Michalowski (1993) model, McKenzie et al. (2007) model and Kozlowski (2007) model have similar formulas, which use exponential equations and consider residual unfrozen water content. The difference is that the Michalowski (1993) model and McKenzie et al. (2007) model only have one fitting parameter, reducing the flexibility of the models, compared to the Kozlowski (2007) model with two fitting parameters. The results in Figure C.1 show that the performance of the Kozlowski (2007) model is better than the Michalowski (1993) model and McKenzie et al. (2007) model. The Anderson and Tice (1972) model and Zhang et al. (2017) model are empirical models with simple equations. These models are easy to apply but have less accuracy. The Anderson and Tice (1972) model prediction approaches infinite when the temperature is close to 0 °C. The Zhang et al. (2017) model is initially proposed for silt and performs well for sand with fines. The performance of Zhang et al. (2017) model is not suitable for sand, clay, and organic soil.

Table 4 summarizes the evaluation results based on Section 3.2 and suggests applications of the seven seismic wave velocity models of permafrost. The time-average model shows a poor prediction among all the models evaluated and may not be suitable for seismic wave velocity predictions in permafrost. And the time-average model cannot predict S-wave velocities.

Table 4. Application of seismic wave velocity models of permafrost based on statistical evaluation

Models	**Prediction Performance**	**Suggested applications**
Time-average model (Wyllie et al., 1958; Timur, 1968)	Overestimate P-wave velocities for all soil types	• Predict P-wave velocity only • Fully frozen permafrost
Zimmerman and King (1986) model	Good performance on P-wave velocity of clay, and S-wave velocity of sand	• Predict S-wave velocity for sand • Predict P-wave velocity for clay
Minshull et al. (1994) model	Overall good performance on both P-wave and S-wave velocities of all soil types	• Predict P-wave and S-wave velocities for sand with fines and clay • Predict P-wave velocity for sand • Predict S-wave velocity for silt

Weighted equation model (Lee et al., 1996)	Good performance on S-wave velocity of silt	• Predict S-wave velocity for silt
Three-phase model (Leclaire et al., 1994)	Good performance on P-wave velocity of silt Good performance on S-wave velocity of clay	• Predict P-wave velocity for silt • Predict S-wave velocity for clay
Biot-Gassmann theory modified by Lee (BGTL) (Lee, 2002)	Good performance on both P-wave and S-wave velocities of sand and clay Good performance on S-wave velocity of sand with fines	• Predict P-wave velocity for sand and clay • Predict S-wave velocity for silt
Dou et al. (2017) model	Overall good performance on both P-wave and S-wave velocities of all soil types	• Predict P-wave and S-wave velocities for sand and clay

In the seismic wave velocity models, the Zimmerman and King (1986) model and BGTL model calculate bulk and shear modulus and then derive V_p and V_s; The Minshull et al. (1994) model and three-phase model calculate V_p and V_s directly; the weighted equation model predicts P-wave velocities first, then derive S-wave velocities based on the empirical relationship between V_p and V_s. Therefore, V_p prediction results are more reliable in the weighted equation model than V_s prediction results. The empirical linear relationship between V_p and V_s for different media varies. S-wave velocity derived by the original weighted equation model depends on the empirical V_p and V_s relationship developed for mudrocks by Castagna et al. (1985) in Equation A.14. This relationship is not suitable for permafrost. In this study, we derive new empirical linear relationship between P-wave and S-wave velocities for unconsolidated permafrost based on large amount of data (369 data points of joint P-wave and S-wave velocities), as presented in Figure 7 and Equation 42. Equation 42 is used for V_s prediction in the weighted equation model to replace the original equation (Equation A.14).

The Zimmerman and King model generally performs better with decreasing unfrozen water content, which corresponding to higher P- and S-wave velocity values. A clear trend can be observed in Figure 5b especially for sand with fines. This is because the Zimmerman and King model assumes a medium unfrozen water content range (less than 60%). However, when ice formation starts as temperature is close to 0 °C, the water phase may be continuous. The Zimmerman and King model may therefore overestimate the seismic wave velocities in most soils as temperature increases.

The Minshull et al. (1994) model is a two-end-member mixing approach, providing an overall good performance for each soil types. The two end-members are mixed to model the intermediate, partially frozen sediment, and the mixing proportions are set to be equal to the relative proportions of pore ice and pore water. Instead of relying on parameter tuning, the mixing proportion is consistent over the full range of the possible ice saturations. However, the mixing scheme of Minshull et al. (1994) cannot apply to unconsolidated sediments because the time-average model (Equation A.1) is used to model the velocities of the fully frozen end-member, the fully unfrozen end-member, and partially frozen condition. Therefore, the Dou et al. (2017) model improves based on the Minshull et al. (1994) model.

In the weighted equation model, Lee et al. (1996) selected $W = 1$ and $n = 1$ to fit the joint P- and S-wave velocities reported by Zimmerman and King (1986). It is challenging to establish the values of W and n for prediction purposes since the values depend on the observed data (Lee et al., 1996; Lee, 2002). $W > 1$ favors the Wood equation (Equation 19) (Nobes et al., 1986). In this study, we selected $W = 1.1$ and $n = 1$.

In the BGTL model, V_{pc}/V_{sc} (the P- and S-wave velocities of the porous solid matrix) is assumed equal to the multiplication of V_p/V_s and the solid fraction for unconsolidated permafrost (Equation A.47), but the actual V_{pc}/V_{sc} is smaller than the value assumed by the BGTL model. Therefore, the BGTL model has relatively low bias but large error in V_s prediction (Figures 6e, C.7e and C.9e). Another error source is from the Biot coefficient estimation. When temperature increases, the S-wave velocity estimated based on the BGTL model is less than the actual measurements for fine-grain soils (Figure 6e).

5. Conclusions

This study evaluates six unfrozen water content models of permafrost. For unfrozen water content estimation, the regression analyses show that semi-empirical models give an overall good performance (average RMSE values are smaller than 5%) when using appropriate fitting parameters. We found that empirical models are easier to apply than theoretical models but lack physical meaning. Empirical models with two fitting parameters perform better compared with models with only one fitting parameter. We proposed a modified and simple semi-empirical model (the modified Dall'Amico's model) for predicting unfrozen water content based on soil temperature.

We also evaluated seven seismic velocity models of permafrost. Regardless of porosity, grain size, and temperature, permafrost of all soil types generally shares the same linear correlation between P-wave and S-wave velocities. We derived the empirical relationship between P-wave and S-wave velocities of permafrost based on large amount of data points. This study evaluates the prediction results of seven seismic wave velocity models based on predicted unfrozen water content using the modified Dall'Amico's model. The statistical evaluation results show that Minshull et al. model and BGTL model have an overall better performance in seismic wave velocity prediction reflected by lower RMSE values than other models. The evaluation performance of the seismic wave velocity models varies with permafrost soil type. The application of each model by soil types of permafrost is summarized in this study.

The unfrozen water content datasets and seismic wave velocity datasets are independent. The unfrozen water content in the seismic wave velocity models is first estimated by the modified Dall'Amico's model, and errors in this estimation may contribute to the estimation accuracy of seismic wave velocity models.

6. Acknowledgments

This study is supported by the National Science Foundation under Grants CMMI-2034363, CMMI-2034366, and ICER-1927718. Dr. Min Liew provided advice on data collection.

7. Author Contribution Statement

Xiaohang Ji: Conceptualization, Methodology, Software, Formal analysis, Investigation, Writing - Original Draft, Visualization **Ming Xiao:** Conceptualization, Methodology, Validation, Writing - Review & Editing, Visualization, Supervision, Project administration, Funding acquisition **Eileen Martin:** Conceptualization, Writing - Review & Editing, Project administration, Funding acquisition **Tieyuan Zhu:** Conceptualization, Writing - Review & Editing, Project administration, Funding acquisition

8. Data Availability Statement

Data for unfrozen water content model evaluation used in this study are available from the original publications: Christ et al., 2009; Li, 2009; Li et al., 2020; Smith and Tice, 1988; McGaw et al., 1983; Oliphant et al., 1983; Aksenov et al., 1998; Hivon and Sego, 1990; Lai et al., 2021; Qiu et al., 2020; Watanabe and Wake, 2009; Zhang et al., 2019; Wen et al., 2012.

Data for seismic wave velocity model evaluation used in this study are available from the original publications: Wang et al., 2006; Christ et al., 2009; Nakano and Arnold, 1973;

Kim et al., 2016; Li, 2009; Meng et al., 2008; Fu et al., 1983; Yang et al., 2015; Ge et al., 2013; Zhang et al., 2018.

All digitized data used in this study are available:

Ji, X., Liew, M., and Xiao, M. 2022. Supplementary data for 'Statistical evaluation of seismic wave velocity models of permafrost'. Penn State Data Commons. http://doi.org/10.26208/6H4X-JC81.

9. Conflict of Interest Statement

No potential conflict of interest was reported by the authors.

References

Aksenov, V.I., Klinova, G.I., and Scheikin, I.V. 1998. Material composition and strength characteristics of saline frozen soils. In Seventh International Conference on Permafrost, Yellow Knife, Canada, 55, 1–4.

Anderson, D.M., and Tice, A.R. 1972. Predicting unfrozen water contents in frozen soils from surface area measurements. Highway Res. Rec. 393, 12–18.

Berryman, J.G. 1995. Mixture theories for rock properties. Rock physics and phase relations: A handbook of physical constants, 3, pp.205–228. https://doi.org/10.1029/RF003p0205.

Biot, M.A. 1956. Theory of propagation of elastic waves in a fluid-saturated porous solid. II. Higher frequency range. The Journal of the Acoustical Society of America, 28(2), pp.179–191. https://doi.org/10.1121/1.1908241.

Carcione, J.M. & Seriani, G. 1998. Seismic and ultrasonic velocities in permafrost. Geophysical Prospecting, 46(4), pp.441–454. https://doi.org/10.1046/j.1365-2478.1998.1000333.x.

Castagna, J.P., Batzle, M.L., and Eastwood, R.L. 1985. Relationships between compressional-wave and shear-wave velocities in clastic silicate rocks. Geophysics, 50(4), pp.571–581. https://doi.org/10.1190/1.1441933.

Christ, M., Kim, Y.C., and Park, J.B. 2009. The influence of temperature and cycles on acoustic and mechanical properties of frozen soils. KSCE Journal of Civil Engineering, 13(3), 153–159. https://doi.org/10.1007/s12205-009-0153-1.

Czurda, K.A., and Hohmann, M. 1997. Freezing effect on shear strength of clayey soils. Applied clay science, 12(1-2), 165–187. https://doi.org/10.1016/S0169-1317(97)00005-7.

Daanen, R.P., Ingeman-Nielsen, T., Marchenko, S.S., Romanovsky, V.E., Foged, N., Stendel, M., Christensen J.H., and Hornbech Svendsen, K. 2011. Permafrost degradation risk zone assessment using simulation models: The Cryosphere, 5, 4, 1043–1056. https://doi.org/10.5194/tc-5-1043-2011.

Dall'Amico, M., Endrizzi, S., Gruber, S., and Rigon, R.J.T.C. 2011. A robust and energy-conserving model of freezing variably-saturated soil. The Cryosphere, 5(2), 469–484.

De Gennes, P.G. 1976. On a relation between percolation theory and the elasticity of gels. Journal de Physique Lettres, 37(1), pp.1–2.

Deschartres, M.H., Cohn-Tenoudji, F., Aguirre-Puente, J., & Khastou, B. 1988. Acoustic and unfrozen water content determination. In Proc. 5th Inl. Conf. on permafrost, 324–328.

Dou, S., Nakagawa, S., Dreger, D., and Ajo-Franklin, J. 2016. A rock-physics investigation of unconsolidated saline permafrost: P-wave properties from laboratory ultrasonic measurements. Geophysics, 81(1), WA233–WA245. https://doi.org/10.1190/geo2015-0176.1.

Dou, S. Nakagawa, S., Dreger, D., and Ajo-Franklin, J.B. 2017. An effective-medium model for P-wave velocities of saturated, unconsolidated saline permafrost. Geophysics, 82(3), EN33–EN50. https://doi.org/10.1190/geo2016-0474.1.

Dvorkin, J., and Nur, A. 1998. Time-average equation revisited. Geophysics, 63(2), 460–464. https://doi.org/10.1190/1.1444347.

Eberhart-Phillips, D., Han, D.H., and Zoback, M.D. 1989. Empirical relationships among seismic velocity, effective pressure, porosity, and clay content in sandstone. Geophysics, 54(1), 82–89. https://doi.org/10.1190/1.1442580.

Ferrero, A.M., Godio, A., Migliazza, M., Sambuelli, L., Segalini, A., and Théodule, A. 2014. Geotechnical and geophysical characterization of frozen granular material. In Landslides in Cold Regions in the Context of Climate Change, 205–218. Springer, Cham. https://doi.org/10.1007/978-3-319-00867-7_15.

Fu R., Zhang J., and Hou Z. 1983. Ultrasonic velocities in frozen soil. In Proc. 4th Inl. Conf. on Permafrost, 311–315.

Gassmann, F. 1951. Elastic waves through a packing of spheres. Geophysics, 16(4), 673–685. https://doi.org/10.1190/1.1437718.

Ge, X., Yang, Z., and Still, B. 2013. Mechanical properties of naturally frozen ice-rich silty soils. In Mechanical Properties of Frozen Soil. ASTM International. https://doi.org/10.1520/STP156820130002.

Guéguen, Y., and Palciauskas, V. 1994. Introduction to the physics of rocks: Princeton University Press.

Hashin, Z., and Shtrikman, S. 1963. A variational approach to the theory of the elastic behaviour of multiphase materials. Journal of the Mechanics and Physics of Solids, 11(2), 127–140. https://doi.org/10.1016/0022-5096(63)90060-7.

Hauck, C., and Mühll, D.V. 2003. Inversion and interpretation of two-dimensional geoelectrical measurements for detecting permafrost in mountainous regions. Permafrost and periglacial processes, 14(4), 305–318. https://doi.org/10.1002/ppp.462.

Hauck, C., Vieira, G., Gruber, S., Blanco, J., and Ramos, M. 2007. Geophysical identification of permafrost in Livingston Island, maritime Antarctica. Journal of Geophysical Research: Earth Surface, 112(F2). https://doi.org/10.1029/2006JF000544.

Haynes, F.D., and Karalius, J.A. 1977. Effect of temperature on the strength of frozen silt (No. 77). Department of Defense, Department of the Army, Corps of Engineers, Cold Regions Research and Engineering Laboratory.

Hill, R. 1952. The elastic behaviour of a crystalline aggregate. Proceedings of the Physical Society. Section A, 65(5), 349. https://doi.org/10.1088/0370-1298/65/5/307.

Hivon, E., and Sego, D.C. 1990. Determination of the unfrozen water content of saline permafrost using time-domain reflectometry (TDR). In Proceedings of the 5th Canadian Permafrost Conference, 257–262. Quebec City, Quebec, Canada: Univ. Laval.

Hoyer, W.A., Simmons, S.O., Spann, M.M., and Watson, A.T. 1975. Evaluation of permafrost with logs. In SPWLA 16th Annual Logging Symposium. OnePetro.

Hu, G., Zhao, L., Zhu, X., Wu, X., Wu, T., Li, R., Xie, C., and Hao, J. 2020. Review of algorithms and parameterizations to determine unfrozen water content in frozen soil. Geoderma, 368, 114277. http://doi.org/10.1016/j.geoderma.2020.114277.

Kim, Y., Chae, D., Kim, K., and Cho, W. 2016. Physical and mechanical characteristics of frozen ground at various sub-zero temperatures. KSCE Journal of Civil Engineering, 20(6), 2365–2374. https://doi.org/10.1007/s12205-015-0542-6.

King, M.S., Zimmerman, R.W., and Corwin, R.F. 1988. Seismic and electrical properties of unconsolidated Permafrost. Geophysical Prospecting, 36(4), 349–364. https://doi.org/10.1111/j.1365-2478.1988.tb02168.x.

Kozlowski, T. 2007. A semi-empirical model for phase composition of water in clay-water systems. Cold Reg. Sci. Technol. 49, 226–236. https://doi.org/10.1016/j.coldregions.2007.03.013.

Kurfurst, P.J. 1976. Ultrasonic wave measurements on frozen soils at permafrost temperatures. Canadian Journal of Earth Sciences, 13(11), 1571–1576. https://doi.org/10.1139/e76-163.

Kuster, G.T., and Toksöz, M.N. 1974. Velocity and attenuation of seismic waves in two-phase media: Part I. Theoretical formulations. Geophysics, 39(5), 587–606. https://doi.org/10.1190/1.1440450.

Lai, Z., Zhao, X., Tang, R., and Yang, J. 2021. Electrical conductivity-based estimation of unfrozen water content in saturated saline frozen sand. Advances in Civil Engineering, 2021. https://doi.org/10.1155/2021/8881304.

Leclaire, P., Cohen-Ténoudji, F., and Aguirre-Puente, J. 1994. Extension of Biot's theory of wave propagation to frozen porous media. The Journal of the Acoustical Society of America, 96(6), 3753–3768. https://doi.org/10.1121/1.411336.

Lee, M.W. 2002. Biot–Gassmann theory for velocities of gas hydrate-bearing sediments. Geophysics, 67(6), 1711–1719. https://doi.org/10.1190/1.1527072.

Lee, M.W., Hutchinson, D.R., Collett, T.S., and Dillon, W.P. 1996. Seismic velocities for hydrate - bearing sediments using weighted equation. Journal of Geophysical Research: Solid Earth, 101(B9), 20347–20358. https://doi.org/10.1029/96JB01886.

Li, H. 2009. Experimental and numerical study of sonic wave propagation in freezing sand and silt. Doctoral Dissertation. University of Alaska Fairbanks, Fairbanks, Alaska.

Li, Z., Chen, J., and Sugimoto, M. 2020. Pulsed NMR measurements of unfrozen water content in partially frozen soil. Journal of Cold Regions Engineering, 34(3), 04020013. https://doi.org/10.1061/(ASCE)CR.1943-5495.0000220.

Liew, M., Ji, X., Xiao, M., Farquharson, L., Nicolsky, D., Romanovsky, V., Bray, M., Zhang, X., and McComb, C. 2022. Synthesis of physical processes of permafrost degradation and geophysical and geomechanical properties of permafrost. Cold Regions Science and Technology, 198, 103522. https://doi.org/10.1016/j.coldregions.2022.103522.

Lu, J., Pei, W., Zhang, X., Bi, J., and Zhao, T. 2019. Evaluation of calculation models for the unfrozen water content of freezing soils. Journal of Hydrology, 575, 976–985. https://doi.org/10.1016/j.jhydrol.2019.05.031.

Lyu, C., Amiri, S.A.G., Grimstad, G., Høyland, K.V., and Ingeman-Nielsen, T. 2020. Comparison of geoacoustic models for unfrozen water content estimation. Journal of Geophysical Research: Solid Earth, 125(10), p.e2020JB019766. https://doi.org/10.1029/2020JB019766.

McGaw, R.W., Berg, R.L., and Ingersoll, J.W. 1983. An investigation of transient processes in an advancing zone of freezing. In Proceedings of Fourth International Conference on Permafrost, Washington, D.C., 821–825.

McKenzie, J.M., Voss, C.I., and Siegel, D.I. 2007. Groundwater flow with energy transport and water–ice phase change: numerical simulations, benchmarks, and application to freezing in peat bogs. Adv. Water Resour. 30 (4), 966–983. https://doi.org/10.1016/j.advwatres.2006.08.008.

Meng, Q., Li, D., Chen, J., Xu, A., and Huang, S. 2008. Experimental research on physical-mechanical characteristics of frozen soil based on ultrasonic technique. In the Ninth International Conference on Permafrost, 2, 1179–1183.

Michalowski, R.L. 1993. A constitutive model of saturated soils for frost heave simulations. Cold Reg. Sci. Technol. 22, 47–63. https://doi.org/10.1016/0165-232X(93)90045-A.

Mindlin, R.D. 1949. Compliance of elastic bodies in contact. Journal of Applied Mechanics, 16, 259–268. https://doi.org/10.1115/1.4009973.

Minshull, T.A., Singh, S.C., and Westbrook, G.K. 1994. Seismic velocity structure at a gas hydrate reflector, offshore western Colombia, from full waveform inversion. Journal of Geophysical Research: Solid Earth, 99(B3), 4715–4734. https://doi.org/10.1029/93JB03282.

Nakano, Y., and Arnold, R. 1973. Acoustic properties of frozen Ottawa sand. Water Resources Research, 9(1), 178–184. https://doi.org/10.1029/WR009i001p00178.

Nakano, Y., and Froula, N.H. 1973. Sound and shock transmission in frozen soils. In Proceedings of the 2nd International Conference on Permafrost, National Academy of Sciences, 359–369.

Nakano, Y., Martin III, R.J., and Smith, M. 1972. Ultrasonic velocities of the dilatational and shear waves in frozen soils. Water Resources Research, 8(4), 1024–1030. https://doi.org/10.1029/WR008i004p01024.

Nobes, D.C., Villinger, H., Davis, E.E., and Law, L.K. 1986. Estimation of marine sediment bulk physical properties at depth from seafloor geophysical measurements. Journal of Geophysical Research: Solid Earth, 91(B14), 14033–14043. https://doi.org/10.1029/JB091iB14p14033.

Oliphant, J.L., Tice, A.R., and Nakano, Y. 1983. Water migration due to a temperature gradient in frozen soil. In Proceedings of Fourth International Conference on Permafrost, Washington, D.C., 951–956.

Pearson, C.F., Halleck, P.M., McGuire, P.L., Hermes, R., and Mathews, M. 1983. Natural gas hydrate deposits: A review of in situ properties. The Journal of

Physical Chemistry, 87(21), 4180–4185. https://doi.org/10.1021/j100244a041.

Qiu, E., Wan, X., Qu, M., Zheng, L., Zhong, C., Gong, F., and Liu, L. 2020. Estimating unfrozen water content in frozen soils based on soil particle distribution. Journal of Cold Regions Engineering, 34(2), 04020002. https://doi.org/10.1061/(ASCE)CR.1943-5495.0000208.

Radd, F.J., and Wolfe, L.H. 1979. Ice lens structures, compression strengths and creep behavior of some synthetic frozen silty soils. In Developments in Geotechnical Engineering, 26, 169–183. Elsevier. https://doi.org/10.1016/B978-0-444-41782-4.50020-8.

Schön, J. 2011. Physical properties of rocks: A workbook (Vol. 8). Elsevier. https://doi.org/10.1016/S1567-8032(11)08009-8.

Smith, M.W., and Tice, A.R. 1988. Measurement of the unfrozen water content of soils. Comparison of NMR (nuclear magnetic resonance) and TDR (time domain reflectometry) methods. Cold Regions Research and Engineering Lab, Hanover, New Hampshire.

Timur, A. 1968. Velocity of compressional waves in porous media at permafrost temperatures. Geophysics, 33, 584–595. https://doi.org/10.1190/1.1439954.

Thimus, J. F., Aguirre-Puente, J., and Cohen-Tenoudji, F. 1991. Determination of unfrozen water content of an overconsolidated clay down to −160°C by sonic approaches-Comparison with classical methods. Ground freezing, 91, 83–88. Rotterdam, Balkema.

van Genuchten, M.T. 1980. A closed-form equation for predicting the hydraulic conductivity of unsaturated soils. Soil science society of America journal, 44(5), 892–898. https://doi.org/10.2136/sssaj1980.03615995004400050002x.

Wang, D.Y., Zhu, Y.L., Ma, W., and Niu, Y.H. 2006. Application of ultrasonic technology for physical–mechanical properties of frozen soils. Cold regions science and technology, 44(1), 12–19. https://doi.org/10.1016/j.coldregions.2005.06.003.

Watanabe, K., and Osada, Y. 2017. Simultaneous measurement of unfrozen water content and hydraulic conductivity of partially frozen soil near 0 C. Cold Regions Science and Technology, 142, 79–84. https://doi.org/10.1016/j.coldregions.2017.08.002.

Watanabe, K., and Wake, T. 2009. Measurement of unfrozen water content and relative permittivity of frozen unsaturated soil using NMR and TDR. Cold Regions Science and Technology, 59(1), 34–41. https://doi.org/10.1016/j.coldregions.2009.05.011.

Wen, Z., Ma, W., Feng, W., Deng, Y., Wang, D., Fan, Z., and Zhou, C. 2012. Experimental study on unfrozen water content and soil matric potential of Qinghai-Tibetan silty clay. Environmental earth sciences, 66(5), 1467–1476. https://doi.org/10.1007/s12665-011-1386-0.

Wood, A.B. 1941. A Textbook of Sound. G. Bell and Sons LTD. London.

Wyllie, M.R.J., Gregory, A.R., and Gardner, G.H.F. 1958. An experimental investigation of factors affecting elastic wave velocities in porous media. Geophysics, 23(3), 459–493. https://doi.org/10.1190/1.1438493.

Yang, Z.J., Still, B., and Ge, X. 2015. Mechanical properties of seasonally frozen and permafrost soils at high strain rate. Cold regions science and technology, 113, 12–19. https://doi.org/10.1016/j.coldregions.2015.02.008.

Zhang, M., Pei, W., Li, S., Lu, J., and Jin, L. 2017. Experimental and numerical analyses of the thermo-mechanical stability of an embankment with shady and sunny slopes in a permafrost region. Applied Thermal Engineering, 127, 1478–1487. https://doi.org/10.1016/j.applthermaleng.2017.08.074.

Zhang, F., Yang, Z.J., Still, B., Wang, J., Yu, H., Zubeck, H., Petersen, T., and Aleshire, L. 2018. Elastic properties of saline permafrost during thawing by bender elements and bending disks. Cold Regions Science and Technology, 146, 60–71. https://doi.org/10.1016/j.coldregions.2017.11.014.

Zhang, M., Zhang, X., Lu, J., Pei, W., and Wang, C. 2019. Analysis of volumetric unfrozen water contents in freezing soils. Experimental Heat Transfer, 32(5), 426–438. https://doi.org/10.1080/08916152.2018.1535528.

Zhu, Y., and Carbee, D.L. 1984. Uniaxial compressive strength of frozen silt under constant deformation rates. Cold regions science and technology, 9(1), 3–15. https://doi.org/10.1016/0165-232X(84)90043-0.

Zimmerman, R.W., and King, M.S. 1986. The effect of the extent of freezing on seismic velocities in unconsolidated permafrost. Geophysics, 51, 1285–1290. https://doi.org/10.1190/1.1442181.

Appendices

Appendix A. Equations of Seismic Wave Velocity Models

(a) Three phase time-average model (Wyllie et al. 1958; Timur 1968):

$$\frac{1}{V_p} = \frac{\phi_w}{V_{pw}} + \frac{\phi_i}{V_{pi}} + \frac{\phi_s}{V_{ps}} \qquad (A.1)$$

where V_{pw}, V_{pi}, V_{ps} are the P-wave velocities of water, ice, and soil solids, respectively.

(b) Zimmerman and King (1986) model

In Zimmerman and King (1986) model, the Kuster-Toksöz (1974) equations are used for the moduli of ice-water mixture, given by

$$\frac{K_h}{K_i} = \frac{1 + \left[\frac{4G_i(K_w - K_i)}{(3K_w + 4G_i)K_i}\right]s}{1 - \left[\frac{3(K_w - K_i)}{3K_w + 4G_i}\right]s} \qquad (A.2)$$

$$\frac{G_h}{G_i} = \frac{(1 - s)(9K_w + 8G_i)}{9K_i + 8G_i + s(6K_i + 12G_i)} \qquad (A.3)$$

where K_h and G_h are bulk and shear modulus of the ice-water mixture, respectively; K_i and G_i are bulk and shear modulus of ice, respectively; K_w is bulk modulus of water, $s = \phi_w/(1 - \phi_s)$ is the water saturation.

Similarly, the bulk (K) and shear (G) moduli of the soil can be obtained using the Kuster-Toksöz equations:

$$\frac{K}{K_h} = \frac{1 + \left[\frac{4G_h(K_s - K_h)}{(3K_s + 4G_h)K_h}\right]\phi_s}{1 - \left[\frac{3(K_s - K_h)}{3K_s + 4G_h}\right]\phi_s} \qquad (A.4)$$

$$\frac{G}{G_h} = \frac{(6K_h + 12G_h)G_s + (9K_h + 8G_h)[(1 - \phi_s)G_h + \phi_s G_s]}{(9K_h + 8G_h)G_h + (6K_h + 12G_h)[(1 - \phi_s)\mu G_s + \phi_s G_h]} \qquad (A.5)$$

where K_s and G_s are bulk and shear modulus of soil solids, respectively.

(c) Minshull et al. (1994) model

In Minshull et al. (1994) model, the P-wave and S-wave velocities of the fully frozen end, i.e., V_{pt} and V_{st} are determined first:

$$\frac{1}{V_{pt}} = \frac{(1 - \phi_s)}{V_{pi}} + \frac{\phi_s}{V_{ps}} \qquad (A.6)$$

$$\frac{1}{V_{st}} = \frac{(1 - \phi_s)}{V_{si}} + \frac{\phi_s}{V_{ss}} \qquad (A.7)$$

where V_{si}, V_{ss} are the S-wave velocities of ice and soil solids, respectively. The corresponding density is $\rho_t = (1 - \phi_s)\rho_i + \phi_s\rho_s$.

Then, the Gassmann's equation is applied to determine the moduli for the fully unfrozen end:

$$K_g - K_{sm} = \frac{\left(1 - \frac{K_{sm}}{K_s}\right)^2}{\frac{1-\phi_s}{K_w} + \frac{\phi_s}{K_s} + \frac{K_{sm}}{K_s^2}} \qquad (A.8)$$

$$G_g = \mu_{sm} \qquad (A.9)$$

where K_g and G_g are the bulk and shear modulus of the water-filled sediment, respectively; K_{sm}, μ_{sm} are the bulk and shear modulus of the porous soil matrix, respectively; K_s and K_w are the bulk modulus of soil solids and water, respectively. The density of the water-filled sediment is $\rho_g = (1-\phi_s)\rho_w + \phi_s\rho_s$.

Finally, P- and S-wave velocities of permaforst are obtained by a weighted average of the slowness of the fully frozen end and fully unfrozen end, using unfrozen water saturation (s) as the mixing ratio:

$$\frac{1}{V_p} = \frac{(1-s)}{V_{pt}} + \frac{s}{V_{pg}} \qquad (A.10)$$

$$\frac{1}{V_s} = \frac{(1-s)}{V_{st}} + \frac{s}{V_{sg}} \qquad (A.11)$$

where V_{pg} and V_{sg} are the P- and S-wave velocities of the water-filled sediment, corresponding to K_g and G_g in Equations A.8 and A.9.

(d) Weighted equation model (Lee et al. 1996)

The weighted equation model (Lee et al. 1996) calculate the weighted average of P-wave velocity based on the three-phase time-average model in Equation A.1 and the Wood equation. The Wood equation calculates the weighted sum of kinetic energy for constituents of water, ice, and soil solids (Lee et al. 1996; Lyu et al. 2020):

$$\frac{1}{\rho {V_{pa}}^2} = \frac{\phi_w}{\rho_w {V_{pw}}^2} + \frac{\phi_i}{\rho_i {V_{pi}}^2} + \frac{\phi_s}{\rho_s {V_{ps}}^2} \qquad (A.12)$$

where V_{pa} is the predicted P-wave velocity, V_{pw}, V_{pi}, V_{ps} are the P-wave velocities of water, ice, and soil solids, respectively.

The weighted equation model by Lee et al. (1996) is

$$\frac{1}{V_p} = \frac{W\phi \cdot s^n}{V_{pa}} + \frac{1 - W\phi \cdot s^n}{V_{pb}} \qquad (A.13)$$

where V_{pb} is the P-wave velocity by time-average equation (Equation A.1), $\phi = \phi_w + \phi_i$ is porosity, unfrozen water saturation $s = \phi_w/\phi$. W is a dimensionless weighting factor. For permafrost, n is a dimensionless constant that simulates the rate of water freezing. An increase in n indicates that the changing rate is faster while freezing.

S-wave velocity V_s in the weighted equation model can be approximately predicted based on an empirical equation for mudrock by Castagna et al. (1985):

$$V_s = 0.8621V_p - 1172.4 \qquad (A.14)$$

(e) Three-phase model (Leclaire et al. 1994)

The resulting equation to calculate P-wave velocity V_{pj} is

$$V_{pj} = \left[Re\left(\sqrt{\Lambda_j}\right)\right]^{-1}, j = 1,2,3 \qquad (A.15)$$

where Re denotes the real part and Λ_j are obtained from the following characteristic equation:

$$A\Lambda^3 - [\rho_{11}B + \rho_{22}C + \rho_{33}D - 2(R_{11}R_{23}\rho_{23} + R_{33}R_{12}\rho_{12})]\Lambda^2 + [bR_{11} + cR_{22} + dR_{33} - 2(\rho_{11}\rho_{23}R_{23} + \rho_{33}\rho_{12}R_{12})]\Lambda - a = 0 \qquad (A.16)$$

The coefficients in Equations A.16 are given in Equation A.19 – A.32.

The S-wave velocity V_{sj} is given by

$$V_{sj} = \left[Re\left(\sqrt{\Omega_j}\right)\right]^{-1}, j = 1,2 \qquad (A.17)$$

where Ω_j is obtained from the second-order equation

$$\Omega^2 \rho_{22}\mu_1\mu_3 - \Omega(\mu_1 b + \mu_3 d) + a = 0 \qquad (A.18)$$

V_{pj} and V_{sj} denote the solutions of Equations A.15 and A.17. The coefficients in Equations A.18 are given in Equation A.30 and A.33 – A.38.

The coefficients of Equation A. 16 and A 18 are provided in Equation A.19 – A.46. Completed procedures and equations can be found in Leclaire et al. (1994).

$$A = R_{11}R_{22}R_{33} - R_{23}^2 R_{11} - R_{12}^2 R_{33} \qquad (A.19)$$

$$B = R_{22}R_{33} - R_{23}^2 \qquad (A.20)$$

$$C = R_{11}R_{33} \qquad (A.21)$$

$$D = R_{11}R_{22} - R_{12}^2 \qquad (A.22)$$

$$R_{11} = [(1 - c_1)\phi_s]^2 K_{av} + K_{sm} \qquad (A.23)$$

$$R_{12} = [(1 - c_1)\phi_s]\phi_w K_{av} \qquad (A.24)$$

$$R_{22} = {\phi_w}^2 K_{av} \qquad (A.25)$$

$$R_{23} = [(1 - c_1)\phi_i]\phi_w K_{av} \qquad (A.26)$$

$$R_{33} = [(1 - c_3)\phi_s]^2 K_{av} + K_{im} \qquad (A.27)$$

$$\rho_{11} = \phi_s \rho_s + (a_{12} - 1)\phi_w \rho_w \qquad (A.28)$$

$$\rho_{12} = -(a_{12} - 1)\phi_w \rho_w \qquad (A.29)$$

$$\rho_{22} = (a_{12} + a_{23} - 1)\phi_w \rho_w \qquad (A.30)$$

$$\rho_{23} = -(a_{23} - 1)\phi_w \rho_w \qquad (A.31)$$

$$\rho_{33} = \phi_i \rho_i + (a_{23} - 1)\phi_w \rho_w \qquad (A.32)$$

$$a = \rho_{11}\rho_{22}\rho_{33} - \rho_{23}^2\rho_{11} - \rho_{12}^2\rho_{33} \qquad (A.33)$$

$$b = \rho_{22}\rho_{33} - \rho_{23}^2 \qquad (A.34)$$

$$c = \rho_{11}\rho_{33} \qquad (A.35)$$

$$d = \rho_{11}\rho_{22} - \rho_{12}^2 \qquad (A.36)$$

$$\mu_1 = [(1 - g_1)\phi_s]^2 \mu_{av} + \mu_{sm} \qquad (A.37)$$

$$\mu_3 = [(1 - g_3)\phi_i]^2 \mu_{av} + \mu_{im} \qquad (A.38)$$

$$b_1 = \eta_D \frac{{\phi_w}^2}{\kappa_s} \qquad (A.39)$$

$$b_2 = \eta_D \frac{{\phi_w}^2}{\kappa_i} \qquad (A.40)$$

$$\kappa_s = \frac{\kappa_{s0}{\phi_w}^3}{(1 - \phi_s)^3} \qquad (A.41)$$

$$\kappa_i = \frac{\kappa_{i0}\left[\frac{1 - \phi_s}{\phi_i}\right]^3}{\left(\frac{\phi_w}{\phi_s}\right)^3} \qquad (A.42)$$

Tortuosity values:

$$a_{12} = \frac{r_{12}(\phi_s \rho)}{\phi_w \rho_w} + 1 \qquad (A.43)$$

$$a_{23} = \frac{r_{23}(\phi_s \rho')}{\phi_w \rho_w} + 1 \qquad (A.44)$$

$$\rho = \frac{\phi_w \rho_w + \phi_i \rho_i}{\phi_w + \phi_i} \qquad (A.45)$$

$$\rho' = \frac{\phi_w \rho_w + \phi_s \rho_s}{\phi_w + \phi_s} \qquad (A.46)$$

(f) Biot-Gassmann theory modified by Lee (BGTL model) (Lee 2002)

In BGTL model, Lee (2002) assumed the relationship of P- and S-wave velocities between soil and its solid skeleton as

$$\frac{V_{pc}}{V_{sc}} = \frac{V_p}{V_s}(1 - \phi_w) \qquad (A.47)$$

where V_{pc}, V_{sc} are the P- and S-wave velocity of the porous solid matrix (soil grains and ice), respectively.

Lee (2002) proposed an empirical relation between the Biot coefficient β and volume proportion of unfrozen water ($\phi_w = \theta_u$) using the weighted equation model:

$$\beta = \frac{-184.0468}{1 + e^{\frac{\phi_w + 0.56468}{0.10817}}} + 0.99494 \qquad (A.48)$$

The Biot coefficient is then used to calculate the modulus, M, which describes the pressure needed to change the fluid volume without changing the total volume based on Gassmann's theory:

$$\frac{1}{M}=\frac{\beta-\phi_w}{K_{sc}}+\frac{\phi_w}{K_w} \qquad (A.49)$$

where K_{sc} is the HS average bulk modulus of the solid matrix (soil grains and ice), and G_{sc} is the corresponding shear modulus.

The bulk modulus K can then be calculated as follows:

$$K=K_{sc}(1-\beta)+\beta^2 M \qquad (A.50)$$

The shear modulus, G, can be estimated from Equations A.46 and A.49:

$$G=\frac{G_{sc}K_{sc}(1-\beta)(1-\phi_w)^2+G_{sc}\beta^2 M(1-\phi_w)^2}{K_{sc}+\frac{4G_{sc}[1-(1-\phi_w)^2]}{3}} \qquad (A.51)$$

(g) Dou et al. (2017) model

The two-end member model by Dou et al. (2017) uses the self-consistent approximation (Berryman, 1995), the Herz-Mindlin contact theory (Mindlin, 1949) and Biot theory (Dou et al. 2017). The fully frozen end consists of soil grains and ice, calculated by self-consistent approximation. The effective moduli of the fully frozen end member (K_{IF} and G_{IF}) are calculated from the following equations:

$$\phi(K_i - K_{IF})P_{*i}^{penny} + (1-\phi)(K_s - K_{IF})P_{*s}^{sphere} = 0 \qquad (A.52)$$

$$\phi(G_i - G_{IF})Q_{*i}^{penny} + (1-\phi)(G_s - G_{IF})Q_{*s}^{sph} \quad = 0 \qquad (A.53)$$

where P_{*i}^{penny}, Q_{*i}^{penny}, P_{*s}^{sphere} and Q_{*s}^{sphere} (unitless) are shape factors calculated based on bulk and shear moduli (Dou et al. 2017).

The fully unfrozen end consists of soil grains and water. The effective moduli of the dry granular frame (K_{sf} and G_{sf}) are first calculated using Hertz-Mindlin contact theory. The effective moduli of the water-filled granular pack (K_{WF} and G_{WF}) are then calculated by

$$K_{WF} = (V_{P\infty}^2 - \frac{4}{3}V_{S\infty}^2)\rho_{WF} \qquad (A.54)$$

$$G_{WF} = V_{S\infty}^2\rho_{WF} \qquad (A.55)$$

where $\rho_{WF} = \rho_s(1-\phi) + \rho_w\phi$, and $V_{P\infty}$ and $V_{S\infty}$ are the high-frequency limiting velocities given by Biot's fluid substitution equations (Dou et al. 2017).

The effective moduli of permafrost are calculated based on modified HS averages as:

$$K = \frac{1}{2}(K_{HS+} + K_{HS-}) \qquad (A.56)$$

$$G = \frac{1}{2}(G_{HS+} + G_{HS-}) \qquad (A.57)$$

$$K_{HS+} = K_{IF} + \frac{s}{(K_{WF} - K_{IF})^{-1} + (1-s)\left(K_{IF} + \frac{4}{3}G_{IF}\right)^{-1}} \quad (A.58)$$

$$G_{HS+} = G_{IF} + \frac{s}{(G_{WF} - G_{IF})^{-1} + 2(1-s)\left(\frac{K_{IF} + 2G_{IF}}{5G_{IF}(K_{IF} + \frac{4}{3}G_{IF})}\right)} \quad (A.59)$$

$$K_{HS} = K_{WF} + \frac{1-s}{(K_{IF} - K_{WF})^{-1} + s\left(K_{WF} + \frac{4}{3}G_{WF}\right)^{-1}} \quad (A.60)$$

$$G_{HS} = G_{WF} + \frac{1-s}{(G_{IF} - G_{WF})^{-1} + 2s\left(\frac{K_{WF} + 2G_{WF}}{5G_{WF}(K_{WF} + \frac{4}{3}G_{WF})}\right)} \quad (A.61)$$

Complete procedures and equations can be found in Dou et al. (2017).

Appendix B. Index properties and testing conditions of the unfrozen water content soil samples

Table B.1 Index properties and testing conditions for unfrozen water content datasets

References	Soil types in figures	USCS or soil description if USCS is not available	Test method	Total moisture content (%)	Porosity (-)	Salinity (ppt)
Christ, 2009	Sand Sand with fines	SP SC ML	Time domain reflectometry	12 12 20	0.28 0.27 0.38	0

	Silt					
Li 2009	Silt	ML	Frequency domain reflectometry sensor; 50 MHz	20, 26	0.43, 0.49	0
Li et al. 2020	Sand Sand with fines Clay	Medium sand Silty clay CL	Pulsed nuclear magnetic resonance	23, 27 20 – 38 20 – 38	0.41, 0.45 0.45 – 0.51 0.42 – 0.46	0
Smith and Tice, 1988	Clay	CL	Nuclear magnetic resonance	33	0.47	0
McGaw et al. 1983	Silt	Silt	Nuclear magnetic resonance	15, 18	0.36	0
Oliphant et al. 1983	Clay	Clay	Nuclear magnetic resonance	22	0.46	0
Aksenov et al. 1998	Clay	Clay	Not reported	48	0.58	1 – 15
Hivon and Sego 1990	Sand Sand with fines	S SM	Time domain reflectometry	17.6 16.5	–	0
Lai et al. 2021	Sand	S	Nuclear magnetic resonance	39	–	0
Qiu et al. 2020	Clay	CL	– (collected from literature)	10 – 32	0.34 – 0.42	0

Watanabe and Wake 2009	Sand Silt Organic soil	S ML OL	Nuclear magnetic resonance	16 – 29 21 – 37 27 – 51	–	0
Zhang et al. 2019	Sand with Fines Silt Clay	SM ML CL	Nuclear magnetic resonance	17 18 9 – 23	0.35 0.38 0.38 – 0.40	0
Wen et al. 2012	Clay	Silty Clay	Nuclear magnetic resonance	16 – 29	–	0

Table B.2. Number of datasets of seismic wave velocities

Soil Types	**Number of Datasets**	**Number of Datapoints**
Sand	14	111
Sand with Fines	9	103
Silt	9	73
Clay	8	48
Organic Soil	1	31
Total	41	369

Table B.3. Index properties and testing conditions for seismic wave velocity datasets

References	Soil types in figures	USCS or soil description if USCS is not available	Test method	Total moisture content (%)	Porosity (-)	Confining pressure (kPa)

Wang et al. 2006	Sand Sand with fines Fine-grained soil	Fine sand SC CL	Ultrasonic; 500 kHz	18 19 31	0.38 0.41 0.45	0
Christ et al. 2009	Sand Sand with fines Fine-grained soil	SP SC ML	Ultrasonic; 2 MHz	12 12 20	0.28 0.27 0.38	0
Nakano and Arnold, 1973	Sand	Medium sand	Ultrasonic; 1 MHz	8 – 22	0.39 – 0.41	0
Zimmerman and King 1986	Sand Fine-grained soil	S ML-CL, CL	Ultrasonic; 500 – 850 kHz	0 – 5 6 – 22	0.36 – 0.40 0.32 – 0.44	350
Kim et al. 2016	Sand Sand with fines	Fine to medium sand SC-SM	Resonant column	19 – 21 8 – 11	0.36 – 0.38 0.26 – 0.27	0
Li 2009	Sand	Fine sand SC ML, silt	Ultrasonic; 400 kHz	30 – 34 20 20 – 36	0.44 – 0.47	0

	Sand with fines Fine-grained soil				0.50 – 0.53 0.43 – 0.49	
King et al. 1982	Sand Fine-grained soil	S C, M	Ultrasonic	22, 25 22 - 29	0.37, 0.40 0.36 – 0.43	340
Meng et al. 2008	Fine-grained soil	CL	Ultrasonic; 50 kHz	11 – 22	0.43	0
Fu et al. 1983	Sand Fine-grained soil	Medium sand C	Ultrasonic	5 – 25	N/A	50
Yang et al. 2015; Ge et al. 2013	Fine-grained soil Organic soil	ML OL	Universal Testing Machine	62 – 141 86 – 225	0.63 – 0.79 0.67 – 0.87	0
Zhang et al. 2018	Sand with Fines Silt	SM ML CL		26 21 – 26 24	0.46 0.40 – 0.46 0.42	0

	Clay					

Table B.4. Elastic moduli and densities of materials

Materials	K (GPa)	G (GPa)	ρ (kg/m^3)
Quartz	44	37	$G_s \cdot \rho_w$
Ice	8.4	3.7	920
Water	2.0	0	1000
Soil matrix (K_{sm} and G_{sm})	1	1	-

Appendix C. Additional statistical evaluation and analysis results of unfrozen water content models and seismic wave velocity models

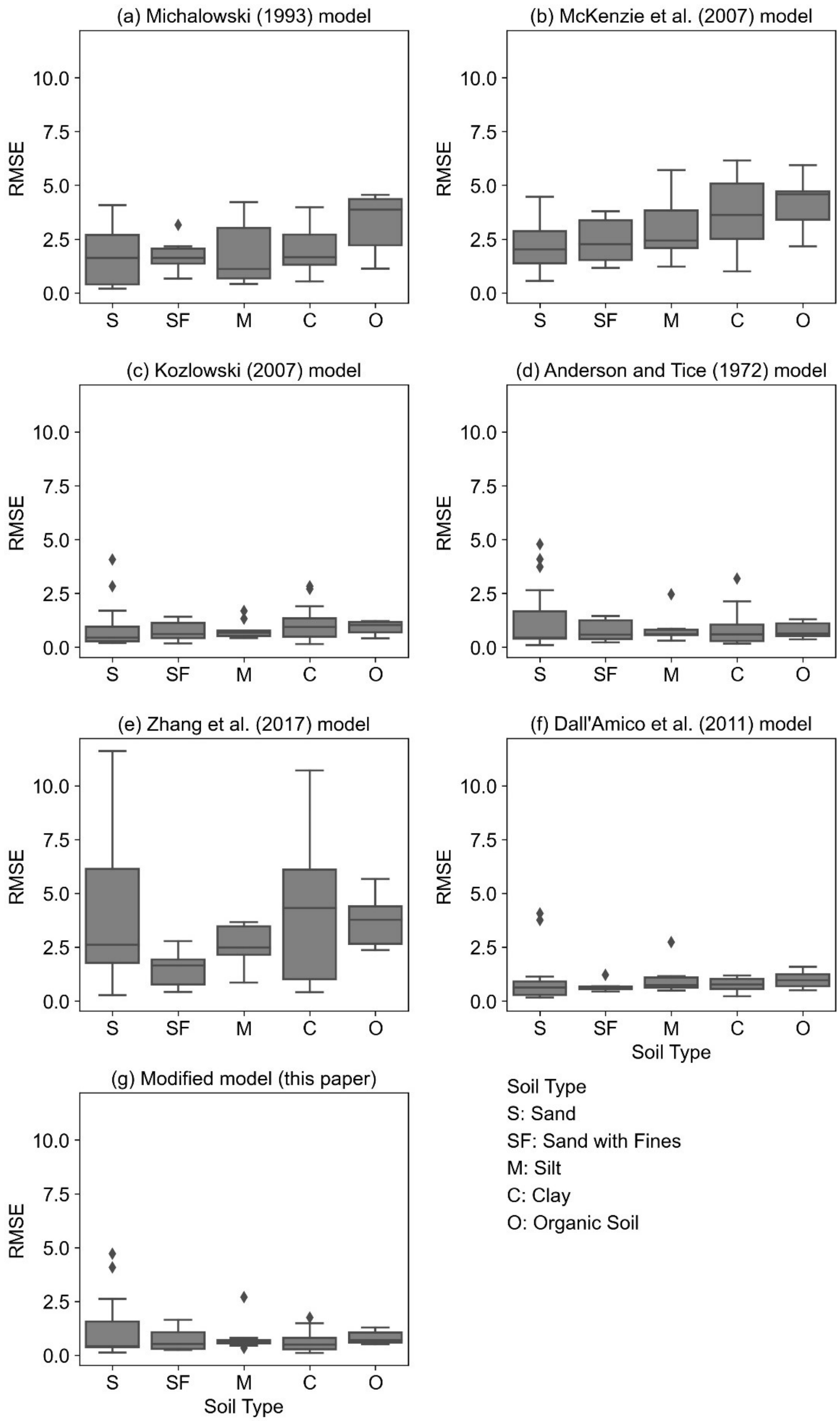

Figure C.1 RMSE of volumetric unfrozen water content models for different soil types

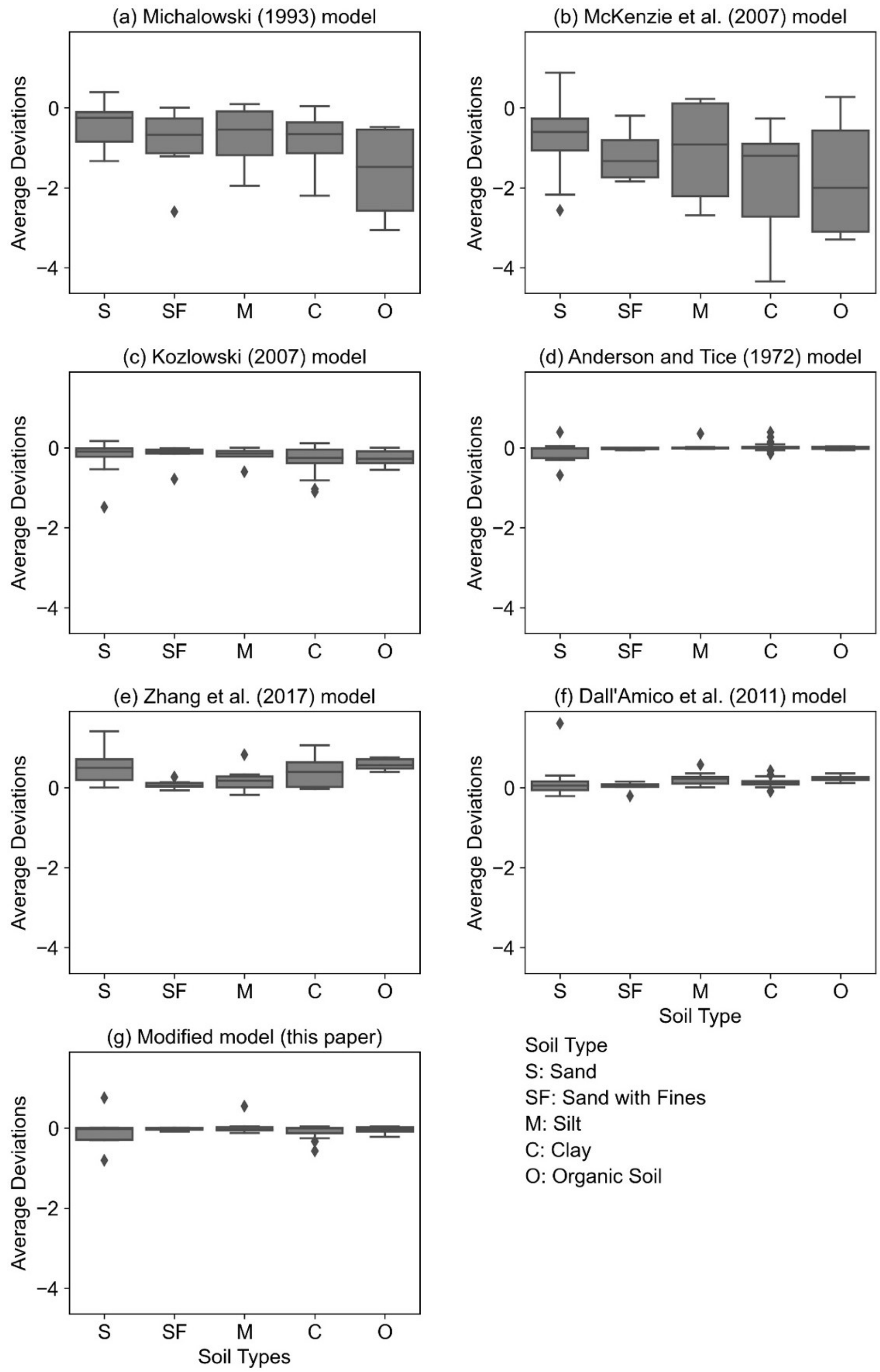

Figure C.2 Average deviations of volumetric unfrozen water content models for different soil types

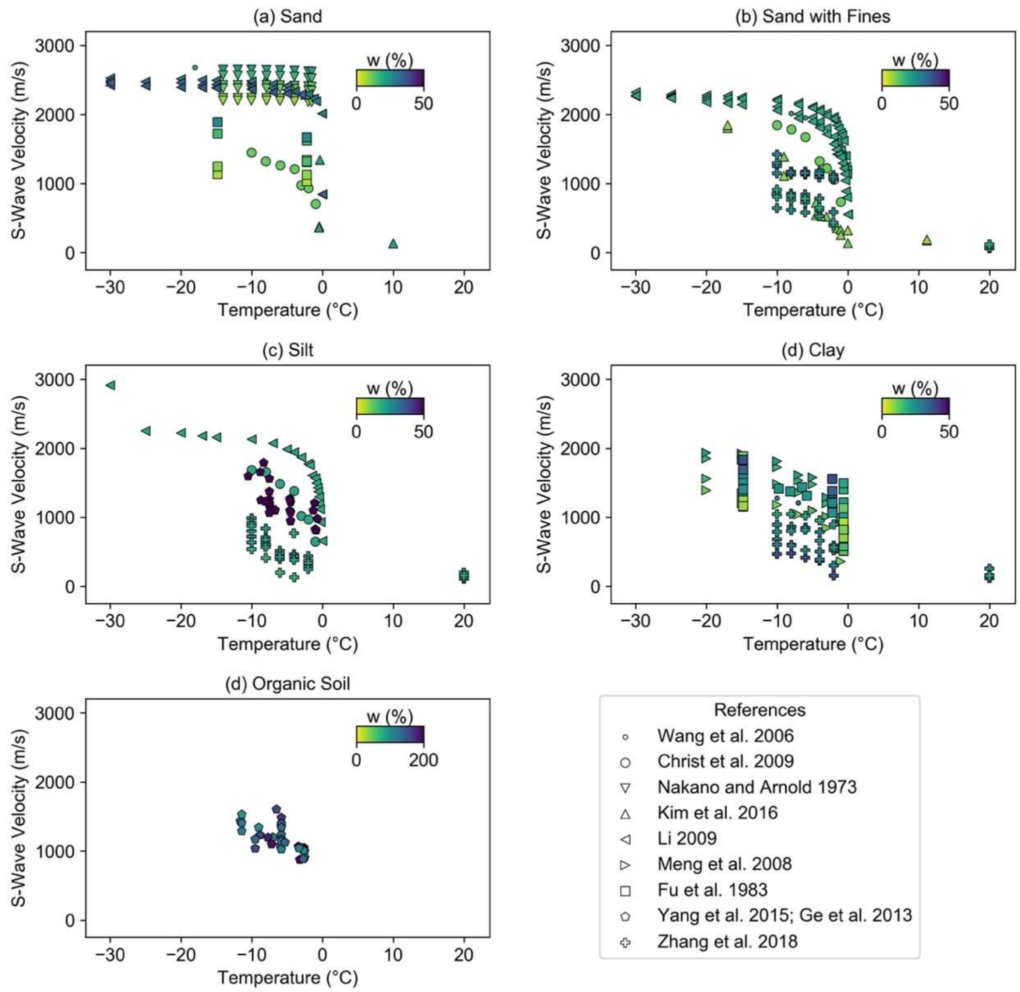

Figure C.3 S-wave velocity data of various soils with temperature

Figures C.4 and C.5 present 5 examples out of 41 datasets of the predicted values of the seven models for P-wave velocities and six models for S-wave velocities for different soil types, including sand, sand with fines, silt, clay, and organic soil. The prediction results from different seismic wave velocity models depend on their theory and assumptions. For example, in Figure 8b, the Zimmerman and King (1986) model shows a good match with sand with fines samples from Li (2009). This sample has initial moisture content $\theta_0 = 27\%$ and porosity $\phi = 0.5$, which align with the application range $\phi \in [0.3, 0.5]$.

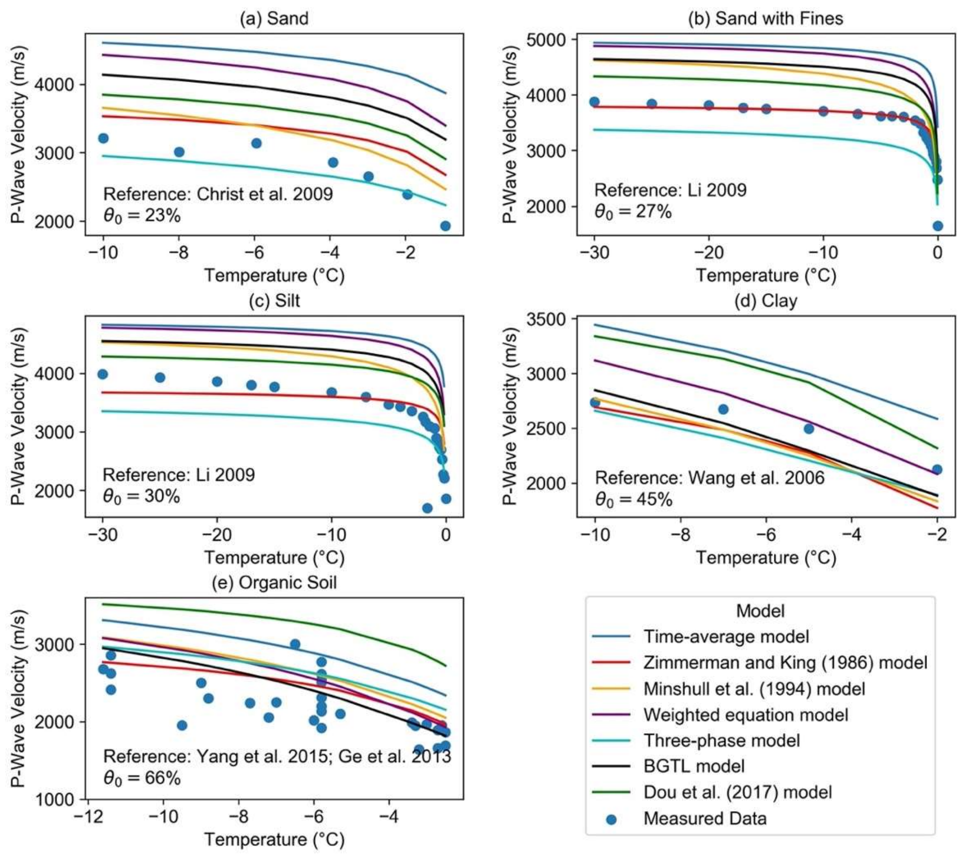

Figure C.4 Seismic wave velocity models for P-wave velocity versus temperature of different soil types

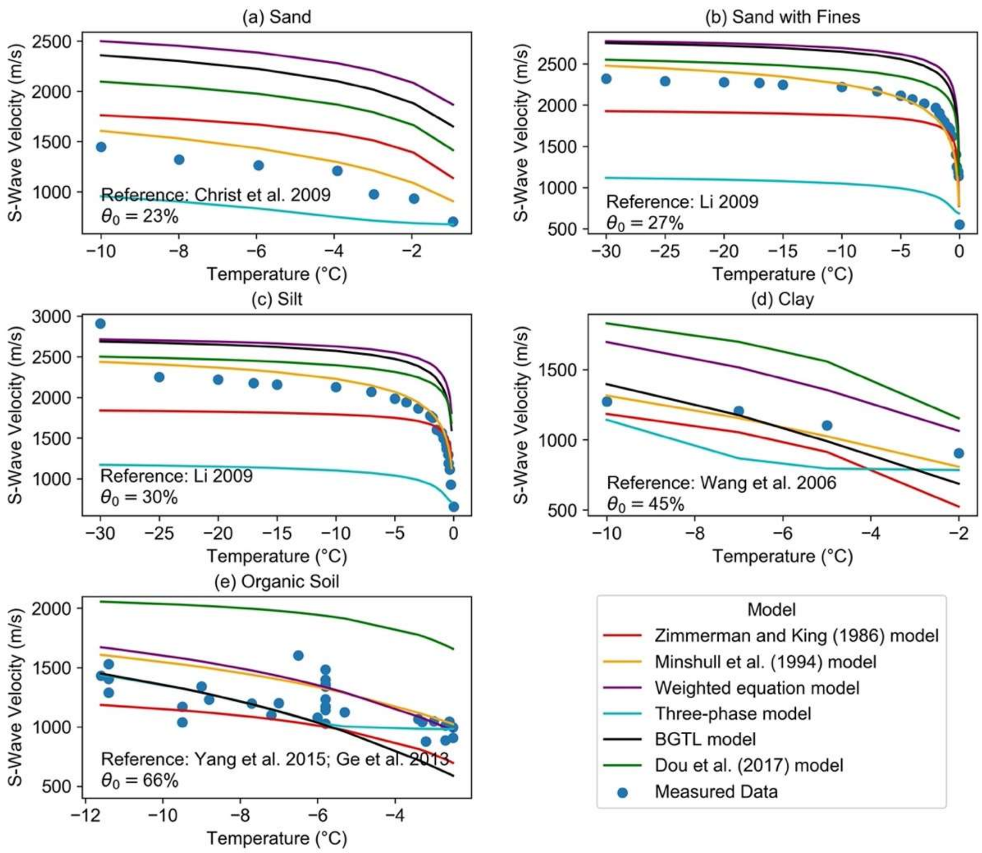

Figure C.5 Seismic wave velocity models for S-wave velocity versus temperature of different soil types

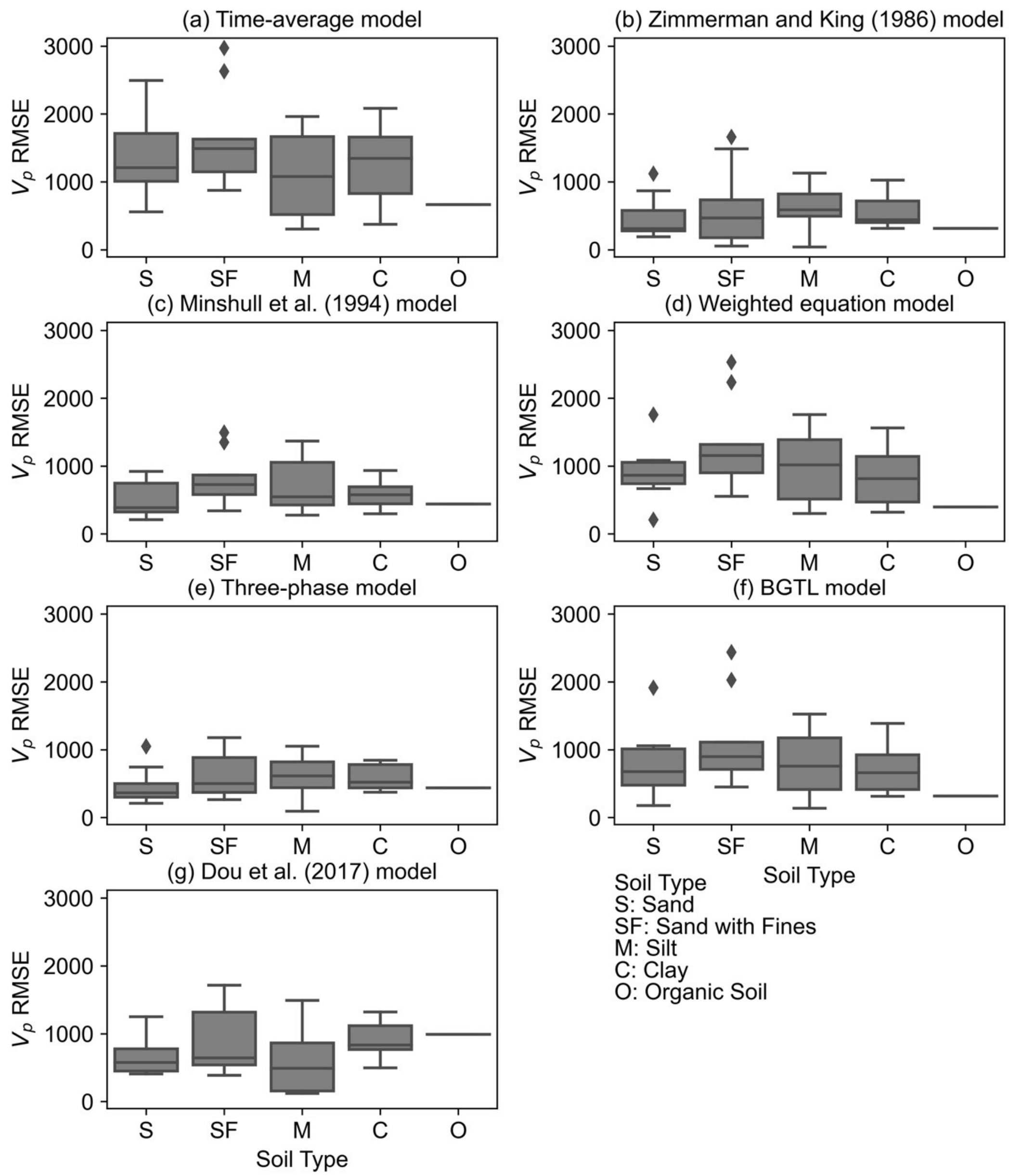

Figure C.6 RMSE of P-wave velocity predictions for different soil types

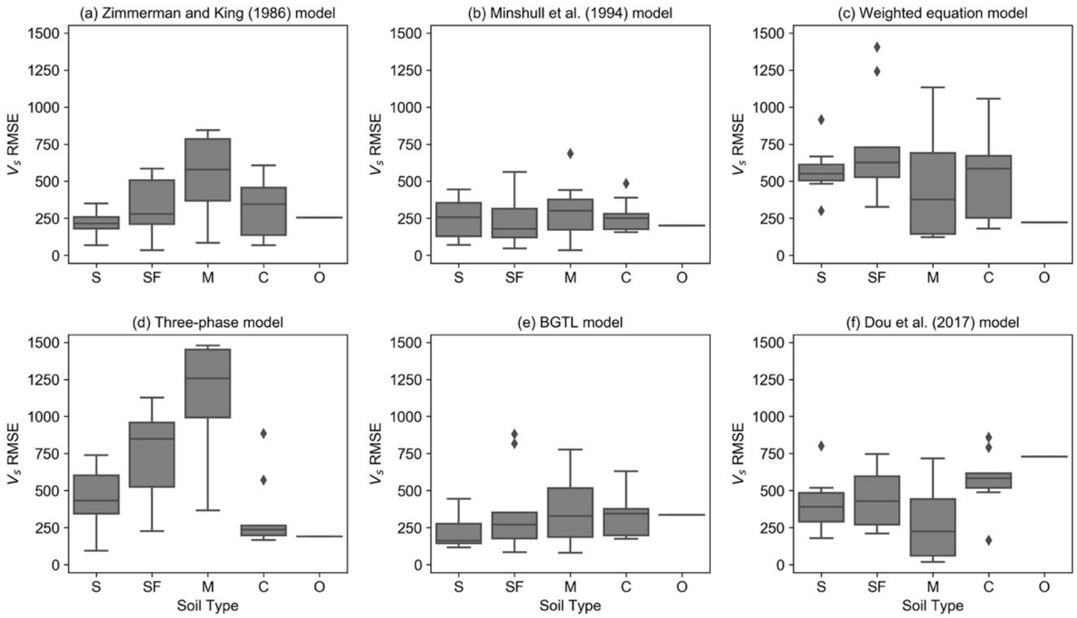

Figure C.7 RMSE of S-wave velocity predictions for different soil types

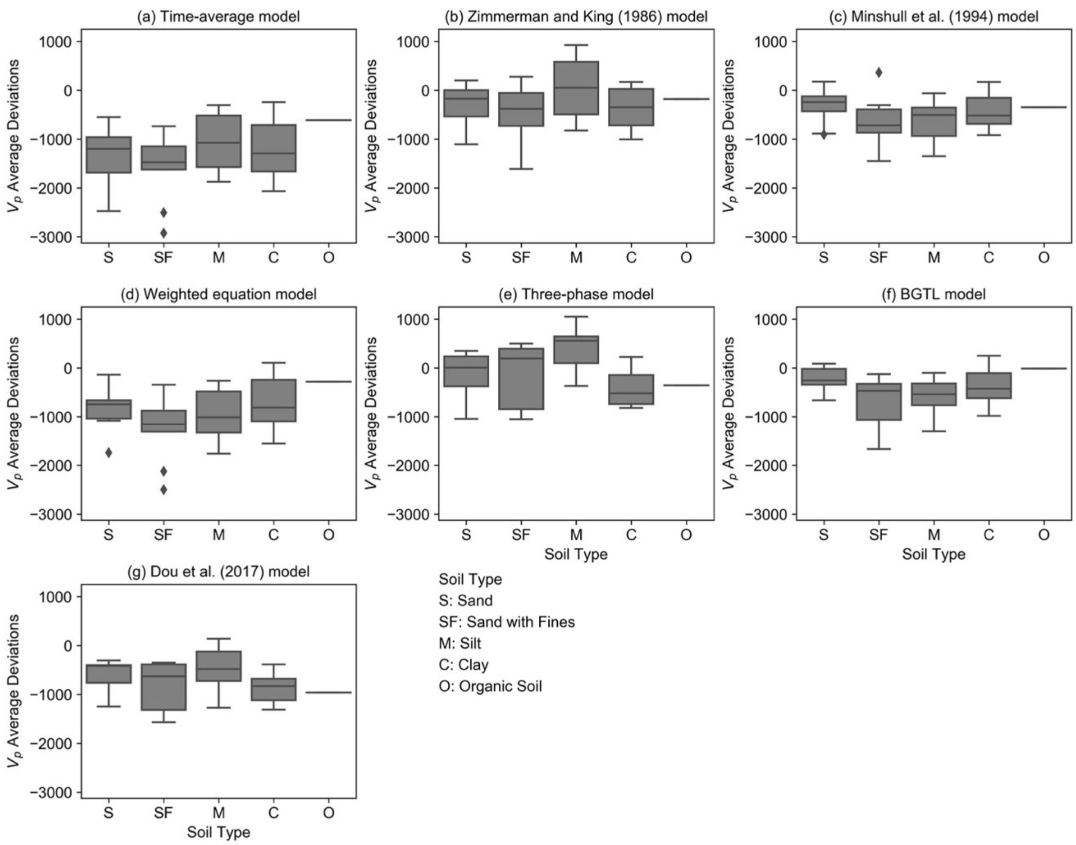

Figure C.8 Average deviations of P-wave velocity predictions by six seismic wave velocity models for different soil types

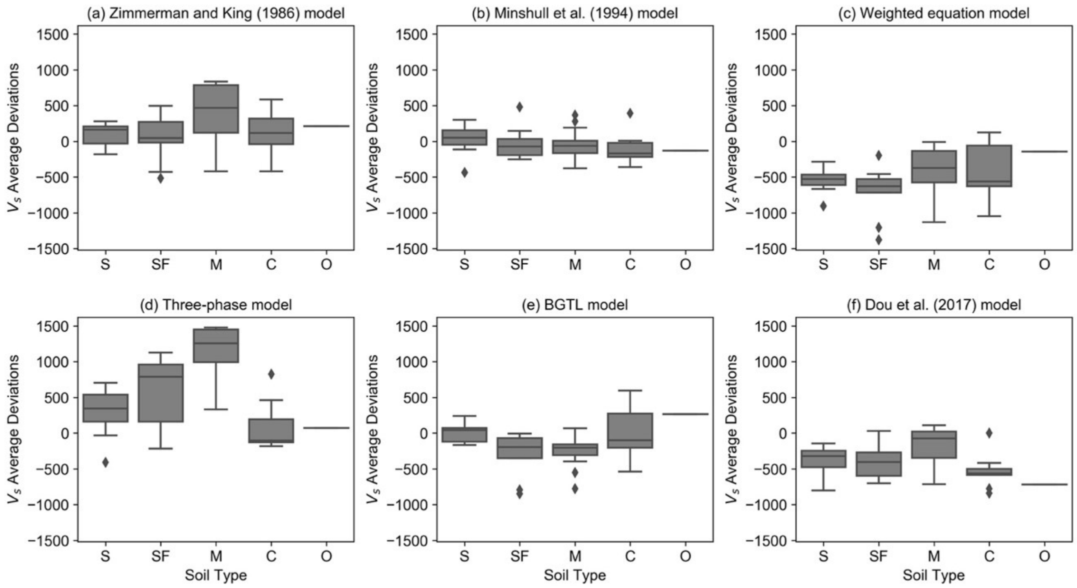

Figure C.9 Average deviations of S-wave velocity predictions by five seismic wave velocity models for different soil types